NASA/CR—2005-213321

Static Aerodynamic Performance Investigation of a Fluid Shield Nozzle

C. Balan and J.W. Askew
General Electric Aircraft Engines, Cincinnati, Ohio

January 2005

The NASA STI Program Office . . . in Profile

Since its founding, NASA has been dedicated to the advancement of aeronautics and space science. The NASA Scientific and Technical Information (STI) Program Office plays a key part in helping NASA maintain this important role.

The NASA STI Program Office is operated by Langley Research Center, the Lead Center for NASA's scientific and technical information. The NASA STI Program Office provides access to the NASA STI Database, the largest collection of aeronautical and space science STI in the world. The Program Office is also NASA's institutional mechanism for disseminating the results of its research and development activities. These results are published by NASA in the NASA STI Report Series, which includes the following report types:

- TECHNICAL PUBLICATION. Reports of completed research or a major significant phase of research that present the results of NASA programs and include extensive data or theoretical analysis. Includes compilations of significant scientific and technical data and information deemed to be of continuing reference value. NASA's counterpart of peer-reviewed formal professional papers but has less stringent limitations on manuscript length and extent of graphic presentations.

- TECHNICAL MEMORANDUM. Scientific and technical findings that are preliminary or of specialized interest, e.g., quick release reports, working papers, and bibliographies that contain minimal annotation. Does not contain extensive analysis.

- CONTRACTOR REPORT. Scientific and technical findings by NASA-sponsored contractors and grantees.

- CONFERENCE PUBLICATION. Collected papers from scientific and technical conferences, symposia, seminars, or other meetings sponsored or cosponsored by NASA.

- SPECIAL PUBLICATION. Scientific, technical, or historical information from NASA programs, projects, and missions, often concerned with subjects having substantial public interest.

- TECHNICAL TRANSLATION. English-language translations of foreign scientific and technical material pertinent to NASA's mission.

Specialized services that complement the STI Program Office's diverse offerings include creating custom thesauri, building customized databases, organizing and publishing research results . . . even providing videos.

For more information about the NASA STI Program Office, see the following:

- Access the NASA STI Program Home Page at ***http://www.sti.nasa.gov***

- E-mail your question via the Internet to help@sti.nasa.gov

- Fax your question to the NASA Access Help Desk at 301–621–0134

- Telephone the NASA Access Help Desk at 301–621–0390

- Write to:
  NASA Access Help Desk
  NASA Center for AeroSpace Information
  7121 Standard Drive
  Hanover, MD 21076

NASA/CR—2005-213321

Static Aerodynamic Performance Investigation of a Fluid Shield Nozzle

C. Balan and J.W. Askew
General Electric Aircraft Engines, Cincinnati, Ohio

Prepared under Contract NAS3–25951

National Aeronautics and
Space Administration

Glenn Research Center

January 2005

Document History

This research was originally published internally as HSR027 in May 1996.

Note that at the time of writing, the NASA Lewis Research Center
was undergoing a name change to the
NASA John H. Glenn Research Center at Lewis Field.
Both names may appear in this report.

Available from

NASA Center for Aerospace Information
7121 Standard Drive
Hanover, MD 21076

National Technical Information Service
5285 Port Royal Road
Springfield, VA 22100

Available electronically at http://gltrs.grc.nasa.gov

Contents

Summary

In pursuit of an acoustically acceptable, high performance exhaust system capable of meeting Federal Aviation Regulation 36 – Stage 3 (FAR 36 Stage 3) noise goals for the High Speed Civil Transport application, General Electric Aircraft Engines conducted a design study to incorporate a fluid shield into a 36–chute suppressor exhaust–nozzle system. After a full scale preliminary mechanical design of the resulting fluid shield exhaust system, scale model aerodynamic performance tests and acoustic tests were conducted to establish both aerodynamic performance and acoustic characteristics. This report presents results from the aerodynamic performance investigation conducted at FluiDyne Engineering Corporation's Channel 14 static thrust stand. The nozzle geometries represented an axisymmetric plug, 36 chute suppressor primary nozzle, with three different plugs (15° solid wall, 15° ten percent porous wall, and a 18° solid wall). In addition to the primary nozzle, four secondary (fluid shield) nozzles, with varying shield heights (thicknesses) of 0.50, 0.60, 0.75, and 1.0 inches, and with shield wrap angles of 180 and 220 degrees, were tested. The tests were conducted at static condition, with a range of primary and secondary nozzle pressure ratios of 1.5 to 4.0 and 1.0 to 3.0, respectively. Data are presented as thrust coefficients, discharge coefficients, chute–base pressure drags, and plug static pressure distributions.

Nozzle static performance at design point nozzle pressure ratio of 3.2 was typically 0.95 for the shield off configurations, and was in the range of 0.88 and 0.91 at the secondary nozzle pressure ratio of 2.2, depending on shield thickness, for the shield on configurations. Fluid shield pressure ratio had a major negative impact on nozzle performance. This reduction in performance was due to a significant increase in chute base pressure drag with the shield flowing. For the configurations and test conditions of this investigations, the impact of plug geometries on the nozzle thrust coefficient was within 0.5 percent. Increasing fluid shield thickness for the same wrap angle improved performance largely due to increased thrust contribution from the unsuppressed shield. Reducing the fluid shield wrap angle, while maintaining constant secondary flow area, improved nozzle performance. This is due to fewer number of chutes being influenced by the shield flow.

Introduction

Environmental acceptability and economic viability are crucial issues in the development of the next generation High Speed Civil Transport (HSCT). Low noise exhaust nozzle technology has significant impact on both issues. The exhaust system design that meets FAR 36 Stage 3 takeoff acoustic requirements and provides high levels of cruise and transonic performance, as well as, adequate takeoff performance at an acceptable weight is essential to the success of the HSCT program.

Takeoff performance characteristics of axisymmetric plug, multi–chute, suppressor nozzles have long been established (References 1, 2, 3, and 4). However, due to their unconventional features, these nozzles have exhibited inefficiencies in thrust coefficient relative to conventional nozzles. On the other hand, takeoff performance characteristics for acoustic shield nozzles (without suppressors) have shown considerable potential (Reference 5).

GE Aircraft Engines (GEAE) has identified an axisymmetric plug, fluid shield nozzle concept that incorporates the perviously demonstrated jet noise.suppression technology of multi–element suppressors (References 1,2, and 3), surrounded by a fluid shield, for reducing jet noise during takeoff operation. The fluid shield nozzle is designed for low specific thrust core engine cycles with jet velocities in the range of 1500 to 2400 feet per second at takeoff flight conditions. This concept requires an extensive data base to develop an understanding of the aerodynamic performance and the aerodynamic mixing effect of the fluid shield with the nozzle core stream. Therefore, an ambient temperature model test was conducted to investigate the static performance of an axisymmetric plug, fluid shield nozzle concept, designed by GE under the NASA Lewis Research Center Task Order Contract NAS3–25951, Task Order #10, "Aero–Propulsion Technology (APT) Research" program. The tests were conducted in FluiDyne Engineering Corporation's Channel 14 static thrust stand during the last quarter of 1992.

Specific objectives of the performance tests were to:

- Establish aerodynamic performance characteristics and design criteria for an axisymmetric plug fluid shield nozzle at the take–off flight condition.

- Quantify the effects of key geometric and aerodynamic variables on performance.

- Evaluate geometric parameter variants consistent with those of the acoustic test program, also conducted under this contract, to understand the effects of potential noise suppression mechanisms on aerodynamic performance.

- Obtain data that can be used later to validate, verify, and correlate Computational Fluid Dynamic (CFD) and other design codes for performance predictions of an axisymmetric plug, fluid shield nozzle.

Test Apparatus and Methods

Static Thrust Stand, Channel 14

Channel 14 is a dual passage, cold flow static thrust stand used to determine aerodynamic performance of exhaust nozzle models. Nozzle thrust is determined from force measurements with a strain–gage force balance. Model air is metered and ducted to the model through two separate passages. Facility overviews are presented in Figures 1 and 2.

The air flows for both the primary and secondary passages of the fluid shield nozzle were obtained from the facility 500 psi dry air storage system. Air for each passage was separately throttled and metered through a long–radius ASME nozzle, ducted to the fluid shield nozzle, and exhausted to the atmosphere. The model assembly was supported by a strain–gage balance and is isolated from the facility piping by two elastic seals; see schematics in Figures 3 and 4. The balance has the capability of measuring three forces (axial and two verticals), from which axial thrust, normal force, and pitching moments were determined.

Facility instrumentation was provided to calculate mass flow rates at Stations 1 and 2, and to calculate the exit thrust produced by the fluid shield nozzle. Details are described later in the Data Reduction Section. Data were recorded using both analog and digital data acquisition systems.

Facility checkout tests were made using a 5.5 inch diameter ASME nozzle to simulate the model primary passage and a 4 inch diameter ASME nozzle to simulate the secondary passage. The expected performance characteristics of the ASME nozzles are defined by equations in Reference 4. Results of the facility checkout are presented in Appendix B.

Operational Procedures

Nozzle model flow conditions were set by independently regulating air flow to the primary and secondary facility meters to obtain the desired Pt_8 and Pt_{18}. Typically, four data points were acquired in a single blow, except for the very high mass flow rate cases. The secondary nozzle (fluid shield) pressure ratio (NPR_s) was held constant during a blow and the primary nozzle pressure ratio ($NPR_{p)}$ was varied over the range of interest. Tests were performed by installing a given fluid shield configuration and testing all three plug combinations for the shield before changing that shield configuration.

Model station notations are shown in Figures 3 and 4 for the ASME checkout nozzles and the fluid shield nozzle, respectively. For these tests the primary flow (model Station 8) was fed by the upper facility meter and the secondary or fluid shield flow (model Station 18) was fed by the lower facility meter.

Model Design and Test Variables

The axisymmetric plug fluid shield nozzle models were designed to represent the take–off flight condition (with noise suppressor chutes deployed) of a GEAE "Fladed Variable Cycle Engine" (Fladed VCE). The nozzle was designed for a primary nozzle pressure ratio of 3.2 and a secondary nozzle pressure ratio of 2.2, at a flight Mach number of 0.32. The baseline fluid shield nozzle was designed with a nominal mass flow rate split of 1.625 to 1 (primary flow to secondary flow). To study the effect of the fluid shield thickness, wrap angle, and mass flow rate on nozzle performance, two shield wrap angles and three shield thickness (gap heights) were tested, see Table I. The fluid shield was varied according to exit flow wrap and exit throat areas. All fluid shields were designed with convergent flow paths (minimum areas at the exit plane). The purpose for evaluating these different fluid shields is that the results may indicate the need for a revision in the flade flow split in the engine cycle.

The close up view of the model assembly is shown in Figure 5. Photographs of various model hardware are given in Figure 6. Figure 6a depicts the four basic shields tested and Figure 6b illustrates the 3 plugs tested. Figure 6c presents a view of the suppressor chutes. Selected test configurations are presented in Figures 7a through 7d and all of the configurations are defined in Table I. A cross section of the fluid shield exhaust system model is given in Figure 8a showing charging station instrumentation and an aft looking forward view of the model assembly is given in Figure 8b along with a schematic of the plug static pressures in Figure 8c.

The primary nozzle contained 36 noise suppressor chutes to reduce noise by dividing the high velocity jet into smaller jets to enhance mixing and thus reducing the jet velocity in a shorter axial length. The primary nozzle throat area remained constant at 21.99 square inches throughout the test program. The primary nozzle flow path was convergent (nozzle throat at the exit plane), and the suppressor area ratio (SAR) was chosen to be 2.5. SAR is defined as the sum of the primary nozzle throat area and the chute area i.e area between the suppressor chutes, divided by the primary nozzle throat area.

Three nozzle plugs, a 15° solid surface, a 15°, 10 percent porous surface, and a 18° solid surface, were tested, to evaluate the effect of primary nozzle plug half–angle and surface porosity on performance. The purpose for the porous plug surface was to weaken the shocks generated by the primary nozzle flow as a mechanism for reducing shock associated noise. By conducting performance tests with the porous plug surface, performance losses associated with the increased surface roughness could be determined. The two plug half–angles were tested to determine plug length effects on performance. A shorter plug length is viewed as a way of reducing the overall weight of a full scale axisymmetric plug nozzle concept.

Instrumentation

The primary charging station instrumentation identified in Figure 8a consisted of 4 rakes with 5 total pressure probes each, and 8 static pressures and 2 thermocouples to measure the

total temperature. The circumferential locations of the total pressure rakes were 0, 90, 180 and 270 degrees. The static pressures were located on the primary duct outer wall at 10, 55 100, 145 190, 235, 280, and 325 degrees. All angles are relative to the 12'o clock position aft looking forward, measured clockwise.

The secondary (fluid shield) charging station instrumentation consisted of 3 rakes with 5 total pressure probes each, 5 wall pressures and two thermocouples. The total pressure rakes were located at 95, 135 and 180 degrees. The static pressures were located on the secondary duct outer wall at 95, 114, 136 158 and 180 degrees.

All of the three nozzle plugs were identically instrumented with 22 static pressure taps, as shown in Figures 8b and 8c. These were divided into two rows, with one row of 10 pressure taps located axially aligned behind a chute base and one row of 12 pressure taps between chutes, in the primary stream. The actual locations of the pressure taps as measured from the suppressor exit plane are given in Table II.

Test Conditions

The primary nozzle pressure ratio varied from 1.5 to 4.0, and the secondary (fluid shield) nozzle pressure ratio varied from jet–off (NPR_S=1.0) to 3.0. Total model flow rates varied from 15.5 to 52.8 pounds–mass per second (lb_m/sec). The primary flow rate varied from 10.0 to 29.0 lb_m/sec depending on the test conditions. Model air flow temperatures were maintained near room temperature conditions of 68°F.

Data Reduction

All data from the instrumentation of the axisymmetric plug fluid nozzle nozzle model and from the Channel 14 facility were recorded and down loaded to a VAX micro computer. Average values of the rake data were used to compute standard performance parameters (e.g., C_{fgr}, C_d, etc.), mass flows, and pressure ratios.

The static axial thrust of an exhaust nozzle is defined as the axial exit momentum of the exhaust flow, plus the difference in exit pressure relative to ambient pressure times the exit area, shown in equation form as:

$$F_x = mv_e + (P_e - P_a)A_e$$

The static thrust measurement used in evaluating the nozzle performance was determined by applying the momentum equation to the control volume shown in Figure 4. The analysis of the forces applied to the control volume includes the entering stream thrusts due to the secondary and primary flows, the balance force corrected for tare forces (B_x), various pressure–area terms, and the axial exit stream thrust.

Summing the axial forces results in the following equation:

$$F_X = m_8 v_1 + P_1 A_1 + P_2(A_2 - A_1) + m_{18} v_{11} + P_{11} A_{11} + P_{12}(A_{12} - A_{11}) - P_a(A_2 + A_{12}) - B_x$$

In the above equation, from continuity the mass flow at station 1 equals station 8 and the mass flow at station 11 equals station 18. The velocities and pressures at station 1 and 11 correspond to that of a choked long radius ASME nozzle throat.

The vertical thrust, F_y, was obtained from the vertical balance force measurements.

$$F_y = B_y$$

The resultant thrust, F_r, was calculated as the vector sum of the axial thrust, F_x, and the vertical thrust, F_y. The nozzle resultant gross thrust coefficient is defined as the ratio of the resultant thrust to the ideal thrust of the primary flow (expanded to ambient) and the ideal thrust of the secondary flow (expanded to ambient), and is shown as;

$$Cfg_r = \frac{F_r}{m_8 V_{i8} + m_{18} V_{i18}} = \frac{(F_x^2 + F_y^2)^{1/2}}{m_8 V_{i8} + m_{18} V_{i18}}$$

The ideal thrust (mv_i) is calculated from the actual mass flow and the dimensionless ideal thrust function based on nozzle pressure ratio.

The resultant thrust vector angle, α, was determined as:

$$\alpha = \tan^{-1}(F_y/F_x)$$

The sign convention for positive values of thrust components and vector angle is defined in Figure 4.

The discharge (flow) coefficient of the nozzle is defined as the ratio of actual flow rate through the nozzle, to the ideal isentropic mass flow rate at the overall nozzle pressure ratio. Overall all nozzle pressure ratios were calculated as $NPR_p = P_{t8}/P_a$ and $NPR_s = P_{t18}/P_a$. For the present tests (exhausting to atmosphere), P_a equals atmospheric pressure.

The discharge coefficients were calculated as:

$$C_{dp} = m_8/m_{8i} \qquad C_{ds} = m_{18}/m_{18i}$$

Detailed data reduction equations and procedures are further discussed in Reference 1.

Results and Discussions

Tabulated performance data are presented in Appendices B and C. Data from this test program are also compiled and documented in Reference 4.

Nozzle Performance Data

The resultant gross thrust coefficients, Cfg_r , are shown in Figure 9, for the three plug configurations tested with varying shield thickness and wrap. Results are presented as a function of primary nozzle pressure ratio, NPR_p , for constant levels of shield pressure ratio, NPR_s . The static performance at design point (NPR_p = 3.2) was typically 0.950 for the shield off configurations (NPR_s = 1.0), and was in the range of 0.880 to 0.910, depending on shield thickness, for the shield on configurations. With the shield off, the observed thrust coefficient levels and trends are consistent with previous chute suppressor plug nozzle test results, Reference 1. However, with the shield operating, $NPR_s > 1$, thrust coefficients decrease significantly by about 4 to 6 points.

The effect of shield parameters on the nozzle performance is illustrated in Figure 10, where thrust coefficients for the 15^0 solid plug are presented as a function of shield pressure ratio. Fluid shield pressure ratio had a major negative impact on nozzle performance, for all of the shield configurations tested. However, at all primary nozzle pressure ratios, for the same wrap angle, increasing the fluid shield thickness improved the performance, as indicated by the 220^0 shield characteristics. This is primarily due to the higher total thrust contribution (higher mass flow) from the unsuppressed shield. Both the 0.6 inch 180^0 shield and the 0.5 inch 220^0 shield had the same shield flow area. A comparison of these two shields indicate that, reducing the fluid shield wrap angle, while maintaining constant flow area, improved nozzle performance. This is due to fewer number of chutes being influenced by the shield flow. The 180^0 shield performs better than the 0.5 inch and 0.75 inch 220^0 shields at all primary nozzle pressure ratios tested. At a primary nozzle pressure ratio of 3.2 (simulated takeoff power) nearly identical performance is obtained by the 220^0, 1.0 inch shield and the 180^0, 0.6 inch shield. The 180^0, 0.6 inch shield influenced fewer suppressor chutes while the 220^0, 1.0 inch shield has higher shield thrust contribution.

The loss in thrust with shield operating is primarily due to the significant increase in the suppressor chute base drag, which is strongly influenced by the shield flow. This is shown by Figure 11 where chute base drag, as a fraction of the ideal gross thrust, is plotted as function of shield pressure ratio, for a primary pressure ratio of 3.2. These data were derived for GEAE Cell41 acoustic tests of the 15^0 porous plug model, conducted under APT Task Order 9. Drag was calculated from static pressure taps installed in the base of the suppressor chutes. Figure 11 indicates that the static pressure on the backsides of the chutes are being pumped down by the shield flow. Also, note that the 180^0 shield had the lowest total drag, due to the fact that fewer suppressor chutes are influenced by the shield flow. This suggests that significant improvements in thrust coefficients for this type of noise suppression concept would require that the suppressor chutes be designed to facilitate turning of the shield flow into the base region, e.g., reducing the chute base angle. However, this would have a major impact on the system mechanical design and may not be a practical solution.

The effect of plug configuration is shown in Figure 12, where thrust coefficients from 15^0 solid, 15^0 porous and 18^0 solid plugs are compared for various shield flows. As can be seen, for the same plug angle, porosity had about 0.5 points negative impact on performance at all flow conditions tested. The effect of plug angle was also similar and the 18^0 solid plug had slightly lower performance than the 15^0 solid plug. Caution, however, should be exercised in drawing conclusions on the effect of plug angle on installed performance based on static data alone, i.e., drag at flight conditions, especially with the suppressor chutes stowed, could be influenced by plug angle. In summary, for the configurations tested, the impact of plug geometry on the nozzle thrust coefficient was within 0.5 percent.

Primary nozzle flow coefficients (Cd_p) are shown in Figure 13 for all of the configurations tested. In general, at primary nozzle pressure ratios less than choking, there is a significant increase in primary flow coefficient with shield flow on relative to the cases with no shield flow. However, for primary nozzle pressure ratios higher than 2.5, the 0.5 inch shield has no effect on the primary nozzle flow coefficient, for all of the three plugs tested. The cases with shield height greater than 0.5 inches indicate moderate suppression due to shield flow for all of the three plugs.

The secondary nozzle flow coefficients (Cd_s) are presented in Figure 14. The secondary flow coefficient levels increased with increasing fluid shield thickness, and were insensitive to both plug angle and primary nozzle pressure ratio.

Static Pressure Data

Static pressure measurements were made along the plug surface for all the fluid shield nozzle configurations. These pressure distributions are presented in Figures 15 through 18. All data are presented as functions of X/L, where X is the distance from the chute exit plane (station 127.242) and L is the plug length (see Figure 8c). Static pressure data are shown as values of P/Pa, the measured local static pressure non–dimensionalized by the measured ambient static pressure. Two rows of static pressure taps were mounted on the nozzle plug surface equally distributed axially (at locations X) from the chute exit plane to the plug tip. One row of static pressures was aligned behind a primary chute base, and one was aligned between chutes, as shown in Figure 8b.

Figure 15 presents plug static pressure distributions for shield flow off cases. In general, these indicate an initial over expansion (lower than ambient) as the flow expands at the chute exit and then a gradual re–compression as the flow continues along the plug. The expansion and compression are well behaved functions of nozzle pressure ratio.

Figure 16 shows plug static pressure distributions with the various shields operating. As can be seen, shield pressure ratio has a strong influence on plug pressures, especially at secondary pressure ratios $NPR_s > 1.5$, indicating a significant interaction between the two flows. Multiple expansions and compressions are evident at high shield and primary pressure ratios. In general, plug static pressure remain above ambient and indicate that the plug is producing positive thrust.

Figure 17 compares design pressure ratio plug pressure distributions for all configurations. Typically, the 18^0 plug exhibited the highest level of re–compression. Plug porosity appears to have very little effect at these conditions. Trends are similar for all shield configurations.

Figure 18 directly compares plug pressure distributions aligned behind the chute base and between chutes, again at design point conditions. Small differences are seen just downstream of the chute exit, however the two distributions rapidly merge indicating a uniform circumferential pressure distribution.

Conclusions

An investigation was conducted in The FluiDyne Engineering Channel 14 static thrust stand facility to determine the effects of fluid shields and plugs on the aerodynamic performance of an axisymmetric plug fluid shield exhaust system. This investigation was conducted at static conditions with varying primary and secondary pressure ratios. Data are presented as thrust coefficients, discharge coefficients, chute base pressure drags, and plug static pressure distributions.

The results of this investigation indicated the following:

1. Nozzle static performance at design point primary nozzle pressure ratio of 3.2 was typically 0.950 for the shield off configurations, and was in the range of 0.880 and 0.910 at the secondary nozzle pressure ratio of 2.2, depending on shield thickness, for the shield on configurations.

2. Fluid shield pressure ratio had a major negative impact on nozzle performance. This reduction in performance was due to a significant increase in chute base pressure drag with the shield flowing.

3. For the configurations and test conditions of this investigations, the impact of plug geometries on the nozzle thrust coefficient was within 0.5 percent.

4. Increasing fluid shield thickness for the same wrap angle improved performance largely due to increased thrust contribution from the unsuppressed shield.

5. Reducing the fluid shield wrap angle, while maintaining constant secondary flow area, improved nozzle performance. This is due to fewer number of chutes being influenced by the shield flow.

This test program has provided an enhanced data base for an advanced jet noise suppressor concept. Results will be helpful in the design of next generation fluid shield jet noise suppressor concepts.

Appendix A
Definition of Symbols

A	Cross–sectional area, in^2
B	Balance Force, lb_f
Cd	Discharge (Flow) coefficient, ratio of measured mass–flow rate to the ideal mass–flow rate
Cfg	Gross thrust coefficient, ratio of the measured nozzle thrust to ideal nozzle thrust
D_{ch}	Chute–base pressure drag, lb_f
F	Thrust, lb_f
fld ht	Fluid shield height (thickness), inches. See Figure 8b
L	Plug length measured from primary nozzle exit plane to plug vertex, inches (see Figure 6b)
M	Mach number
m	Mass flow rate, slugs/sec
NPR	Nozzle pressure ratio, P_t/P_a
P	Pressure, psia
SAR	Suppressor area ratio – $(A_7 + A_{ch})/A_7$, Where A_7 is primary nozzle throat area and A_{ch} is the area between the suppressor chutes at suppressor exit
T	Temperature, ^0R
v	Velocity, ft/sec
wrap	circumferential extent of fluid shield, degrees (see Figure 8b.)
X	Axial distance down stream of the primary nozzle exit, inches
α	Thrust vector angle, degree
Δ	Incremental quantity

Subscripts

a	Ambient or free–stream
ch	Suppressor Chute
e	Nozzle Exit
i	Ideal
p	Primary flow
r	Resultant
s	Secondary flow
t	Total conditions
x	Axial
y	Vertical
1	ASME flow measuring Nozzle Throat (Primary Flow)
2	Primary Flow Flexible Seal
8	Test Nozzle Primary Flow Throat
11	ASME flow measuring Nozzle Throat (Secondary Flow)
12	Secondary Flow Flexible Seal
18	Test Nozzle Secondary (Fluid Shield) Flow Throat

Appendix B
ASME Checkout Nozzle Test

PRIMARY ONLY TEST DATA
5.5 inch ASME Nozzle (6070–076)

Data Point #	NPR_p	C_{fgp}	C_{dp}
PRE – TEST			
804.01	3.994	0.9818	0.9921
804.02	3.988	0.9818	0.9921
804.03	3.997	0.9818	0.9929
803.01	3.190	0.9901	0.9918
803.02	3.193	0.9900	0.9918
803.03	2.991	0.9914	0.9922
802.01	2.492	0.9953	0.9912
802.02	2.495	0.9952	0.9912
802.03	2.487	0.9948	0.9915
801.02	1.993	0.9951	0.9908
801.03	1.992	0.9949	0.9907
801.04	1.982	0.9944	0.9913
800.01	1.493	0.9926	0.9885
800.02	1.495	0.9928	0.9888
800.03	1.486	0.9915	0.9893
POST – TEST			
815.01	3.996	0.9816	0.9924
815.02	3.999	0.9818	0.9925
814.01	3.196	0.9897	0.9917
814.02	3.194	0.9900	0.9920
813.01	2.496	0.9947	0.9910
813.02	2.501	0.9951	0.9911
812.01	1.992	0.9944	0.9908
812.02	1.993	0.9949	0.9908
811.01	1.496	0.9923	0.9886
811.02	1.497	0.9943	0.9892

DUAL FLOW TEST DATA

5.5 inch ASME Nozzle (6070–076) – primary

4.0 inch ASME Nozzle (6051–4232) – secondary

Data Point #	NPR_p	NPR_s	C_{fg}	C_{dp}	C_{ds}
PRE – TEST					
809.01	3.991	4.018	0.9813	0.9923	0.9923
809.02	3.995	4.019	0.9815	0.9924	0.9922
808.01	3.002	3.014	0.9910	0.9921	0.9920
808.02	2.994	3.012	0.9912	0.9915	0.9917
807.01	2.503	2.513	0.9942	0.9912	0.9908
807.02	2.499	2.510	0.9944	0.9912	0.9911
806.01	1.998	2.007	0.9943	0.9908	0.9908
806.02	2.000	2.006	0.9943	0.9907	0.9906
805.01	1.502	1.503	0.9913	0.9890	0.9902
805.02	1.501	1.504	0.9912	0.9887	0.9900
POST – TEST					
555.01	2.002	1.998	0.9951	0.9911	0.9906
820.01	3.994	4.024	0.9816	0.9926	0.9925
819.01	2.993	3.020	0.9911	0.9917	0.9918
818.01	2.493	2.519	0.9941	0.9912	0.9913
817.01	1.997	2.010	0.9940	0.9910	0.9907
816.01	1.497	1.505	0.9914	0.9893	0.9901
555.02	1.996	2.051	0.9947	0.9906	0.9910
820.02	3.981	4.022	0.9813	0.9923	0.9927
819.02	2.986	3.014	0.9909	0.9917	0.9918
818.02	2.484	2.511	0.9937	0.9911	0.9913
817.02	1.988	2.010	0.9934	0.9902	0.9906
816.02	1.490	1.506	0.9899	0.9884	0.9896
820.03	3.987	4.019	0.9811	0.9925	0.9921
819.03	2.984	3.019	0.9909	0.9917	0.9915
818.03	2.491	2.511	0.9943	0.9911	0.9909
817.03	1.989	2.018	0.9941	0.9901	0.9901
816.03	1.489	1.509	0.9915	0.9881	0.9893

Appendix C

Tabulation of Nozzle Performance Data

Primary Only Tests

Config.	Data Point	NPR_p	C_{fgr}	C_{fgx}	C_{fgy}	α degrees	C_{dp}
PRIMARY ONLY TEST							
111	12.01	3.993	.9537	.9537	.0007	.04	.9661
	12.02	3.189	.9569	.9569	.0004	.02	.9635
	12.03	2.492	.9544	.9544	.0003	.02	.9610
	12.04	1.497	.9385	.9385	.0006	.03	.9571
211	18.01	3.998	.9499	.9499	–.0003	–.02	.9672
	18.02	3.185	.9527	.9527	–.0003	–.02	.9641
	18.03	2.487	.9507	.9507	.0004	.02	.9614
	18.04	1.495	.9356	.9356	.0004	.03	.9562
311	22.01	3.998	.9514	.9514	–.0003	–.02	.9664
	22.02	3.202	.9549	.9549	–.0004	–.03	.9641
	22.03	2.503	.9531	.9531	–.0002	–.01	.9614
	22.04	1.508	.9374	.9374	–.0013	–.08	.9596
MID – TEST							
312	35.01	3.983	.9523	.9523	.0000	.00	.9651
	35.02	3.192	.9555	.9555	–.0010	–.06	.9625
	35.03	2.495	.9536	.9536	–.0017	–.10	.9593
	35.04	1.500	.9366	.9366	–.0004	–.02	.9570
312	36.01	3.986	.9526	.9526	–.0003	–.02	.9653
	36.02	3.194	.9560	.9560	–.0012	–.07	.9630
	36.03	2.497	.9539	.9539	–.0010	–.06	.9598
	36.04	1.500	.9371	.9371	–.0012	–.07	.9574
POST – TEST							
324	61.01	4.013	.9529	.9529	–.0002	–.01	.9630
	61.02	3.213	.9564	.9564	–.0009	–.05	.9605
	61.03	2.509	.9548	.9548	–.0011	–.07	.9576
	61.04	1.518	.9375	.9375	–.0003	–.02	.9546

Tabulation Of Nozzle Performance Data
Dual Flow Tests

Config.	Data Point	NPR_p	NPR_s	C_{fgr}	C_{fgx}	C_{fgy}	α degree	C_{dp}	C_{ds}
111	13.01	3.973	3.001	.9058	.9051	.0348	2.20	.9661	.9777
	13.02	3.187	3.002	.8927	.8917	.0416	2.67	.9639	.9781
	13.03	2.489	3.003	.8834	.8820	.0489	3.18	.9609	.9789
	13.04	1.498	3.000	.8814	.8786	.0706	4.59	.9798	.9792
	10.01	3.980	2.204	.9105	.9101	.0255	1.61	.9659	.9765
	10.02	3.187	2.201	.8991	.8986	.0299	1.91	.9535	.9767
	10.03	2.487	2.200	.8892	.8884	.0377	2.43	.9612	.9770
	10.04	1.494	2.201	.8713	.8691	.0615	4.05	.9789	.9776
	11.01	3.981	1.503	.9251	.9250	.0144	0.89	.9660	.9539
	11.02	3.187	1.497	.9190	.9188	.0183	1.14	.9635	.9539
	11.03	2.491	1.499	.9067	.9064	.0245	1.55	.9611	.9543
	11.04	1.494	1.501	.8651	.8640	.0451	2.99	.9739	.9549
211	15.01	3.980	3.018	.9028	.9022	.0335	2.13	.9661	.9780
	15.02	3.189	2.995	.8886	.8877	.0392	2.53	.9632	.9783
	15.03	2.485	2.998	.8771	.8759	.0465	3.04	.9604	.9784
	15.04	1.498	2.997	.8765	.8737	.0704	4.61	.9792	.9788
	16.01	3.980	2.208	.9068	.9065	.0249	1.58	.9663	.9762
	16.02	3.182	2.205	.8943	.8938	.0286	1.83	.9634	.9766
	16.03	2.491	2.201	.8831	.8834	.0354	2.30	.9608	.9769
	16.04	1.500	2.206	.8657	.8635	.0616	4.08	.9780	.9775
	17.01	3.981	1.507	.9214	.9213	.0136	0.85	.9668	.9541
	17.02	3.181	1.501	.9156	.9154	.0168	1.05	.9637	.9540
	17.03	2.486	1.500	.9026	.9023	.0231	1.47	.9609	.9544
	17.04	1.495	1.500	.8597	.8585	.0445	2.97	.9736	.9551
311	19.01	3.993	3.013	.9038	.9029	.0387	2.45	.9666	.9782
	19.02	3.196	3.011	.8900	.8888	.0463	2.98	.9646	.9787
	19.03	2.501	3.012	.8782	.8765	.0550	3.59	.9616	.9788
	19.04	1.504	3.011	.8767	.8731	.0801	5.24	.9812	.9791

Tabulation Of Nozzle Performance Data
Dual Flow Tests – Continued (continued)

Config.	Data Point	NPR_p	NPR_s	C_{fgr}	C_{fgx}	C_{fgy}	α degree	C_{dp}	C_{ds}
311	20.01	3.992	2.202	.9083	.9078	.0290	1.83	.9664	.9767
	20.02	3.196	2.210	.8963	.8957	.0329	2.11	.9644	.9769
	20.03	2.501	2.207	.8855	.8846	.0419	2.71	.9618	.9771
	20.04	1.504	2.202	.8672	.8644	.0695	4.60	.9806	.9774
	21.01	3.995	1.503	.9227	.9225	.0161	1.00	.9664	.9543
	21.02	3.200	1.504	.9165	.9163	.0190	1.19	.9642	.9547
	21.03	2.499	1.501	.9044	.9041	.0261	1.65	.9619	.9549
	21.04	1.499	1.503	.8626	.8612	.0487	3.24	.9758	.9553
112	32.01	3.998	3.008	.9144	.9134	.0441	2.76	.9628	.9883
	32.01	3.185	3.009	.9052	.9037	.0507	3.21	.9602	.9886
	32.03	2.489	3.009	.9053	.9035	.0573	3.63	.9577	.9883
	32.04	1.498	3.009	.9081	.9054	.0705	4.45	.9771	.9891
	33.01	3.986	2.212	.9108	.9102	.0339	2.13	.9627	.9866
	33.02	3.187	2.206	.8999	.8990	.0383	2.44	.9603	.9872
	33.03	2.495	2.205	.8964	.8953	.0459	2.94	.9576	.9869
	33.04	1.501	2.203	.8935	.8911	.0659	4.23	.9761	.9874
	34.01	3.990	1.506	.9239	.9237	.0194	1.20	.9630	.9644
	34.02	3.186	1.503	.9170	.9167	.0243	1.52	.9604	.9645
	34.03	2.492	1.502	.9068	.9063	.0320	2.02	.9579	.9645
	34.04	1.496	1.503	.8813	.8796	.0546	3.55	.9720	.9653
212	31.01	3.978	3.020	.9099	.9089	.0436	2.74	.9657	.9876
	31.02	3.184	3.009	.8996	.8983	.0498	3.17	.9636	.9883
	31.03	2.490	3.019	.8980	.8980	.0561	3.57	.9604	.9886
	31.04	1.497	3.012	.9048	.9021	.0701	4.44	.9799	.9890
	30.01	4.012	2.209	.9073	.9067	.0330	2.08	.9667	.9867
	30.02	3.207	2.207	.8952	.8945	.0372	2.38	.9643	.98709
	30.03	2.505	2.209	.8902	.8891	.0441	2.84	.9613	.9871
	30.04	1.503	2.206	.8899	.8875	.0657	4.23	.9787	.9874

Tabulation Of Nozzle Performance Data
Dual Flow Tests (continued)

Config.	Data Point	NPR_p	NPR_s	C_{fgr}	C_{fgx}	C_{fgy}	α degree	C_{dp}	C_{ds}
212	29.01	3.994	1.507	.9204	.9202	.0193	1.20	.9659	.9648
	29.02	3.190	1.502	.9135	.9132	.0241	1.51	.9632	.9644
	29.03	2.495	1.504	.9031	.9026	.0309	1.96	.9609	.9649
	29.04	1.496	1.502	.8768	.8752	.0534	3.49	.9750	.9650
312	23.01	4.000	3.082	.9115	.9102	.0494	3.11	.9655	.9878
	23.02	3.194	3.008	.9029	.9012	.0562	3.57	.9633	.9884
	23.03	2.498	3.009	.9012	.8989	.0644	4.10	.9610	.9885
	23.04	1.511	3.019	.9037	.9004	.0772	4.90	.9801	.9887
	24.01	3.994	2.211	.9081	.9073	.0381	2.41	.9661	.9853
	24.02	3.200	2.204	.8973	.8963	.0428	2.74	.9643	.9861
	24.03	2.497	2.206	.8922	.8907	.0517	3.32	.9618	.9862
	24.04	1.508	2.204	.8892	.8863	.0729	4.70	.9805	.9866
	25.01	4.028	1.505	.9216	.9213	.0227	1.41	.9680	.9640
	25.02	3.219	1.504	.9140	.9136	.0275	1.73	.9657	.9645
	25.03	2.519	1.502	.9041	.9034	.0363	2.30	.9627	.9645
	25.04	1.515	1.501	.8781	.8760	.0603	3.94	.9766	.9647
113	47.01	3.999	3.012	.9124	.9112	.0448	2.82	.9641	.9978
	48.01	3.211	3.021	.9062	.9048	.0513	3.25	.9610	.9977
	47.02	2.504	3.008	.9086	.9071	.0521	3.29	.9584	.9983
	49.02	1.509	3.017	.9128	.9111	.0544	3.42	.9767	.9984
	46.01	4.004	2.210	.9165	.9157	.0381	2.38	.9632	.9960
	46.02	3.205	2.205	.9068	.9057	.0440	2.78	.9604	.9963
	46.03	2.509	2.211	.9052	.9038	.0500	3.17	.9581	.9963
	46.04	1.506	2.211	.9062	.9039	.0639	4.04	.9760	.9965
	45.01	3.998	1.506	.9249	.9246	.0246	1.43	.9624	.9740
	45.02	3.202	1.504	.9193	.9188	.0305	1.90	.9607	.9740
	45.03	2.505	1.503	.9114	.9106	.0388	2.44	.9578	.9741
	45.04	1.503	1.501	.8950	.8930	.0585	3.74	.9725	.9743

Tabulation Of Nozzle Performance Data
Dual Flow Tests (continued)

Config.	Data Point	NPR_p	NPR_s	C_{fgr}	C_{fgx}	C_{fgy}	α degree	C_{dp}	C_{ds}
213	44.01	4.013	3.018	.9076	.9066	.0443	2.80	.9647	.9970
	43.01	3.214	3.010	.9031	.9016	.0514	3..26	.9612	.9976
	44.02	2.506	3.009	.9056	.9042	.0512	3.24	.9593	.979
	43.02	1.509	2.991	.9103	.9086	.0551	3.47	.9770	.9981
	42.01	4.005	2.205	.9127	.9119	.0376	2.36	.9642	.9963
	42.02	3.209	2.211	.9034	.9024	.0429	2.72	.9621	.9964
	42.03	2.508	2.210	.9002	.8989	.0486	3.09	.9593	.9962
	42.04	1.505	2.218	.9049	.9027	.0631	4.00	.9772	.9970
	41.01	4.007	1.509	.9218	.9214	.0248	1.54	.9643	.9749
	41.02	3.206	1.505	.9154	.9149	.0299	1.87	.9616	.9750
	41.03	2.501	1.504	.9075	.9067	.0374	2.36	.9590	.9755
	41.04	1.504	1.504	.8912	.8894	.0574	3.69	.9739	.9755
313	38.01	3.992	3.018	.9098	.9085	.0502	3.16	.9655	.9977
	38.02	3.191	3.005	.9031	.9012	.0580	3.68	.9629	.9982
	39.01	2.500	3.008	.9051	.9032	.0594	3.76	.9592	.9978
	39.02	1.506	3.009	.9100	.9081	.0586	3.69	.9799	.9988
	37.01	3.983	2.208	.9149	.9138	.0430	2.69	.9646	.9964
	37.02	3.189	2.207	.9050	.9036	.0493	3.12	.9625	.9965
	37.03	2.497	2.206	.9023	.9006	.0563	3.58	.9600	.9970
	37.04	1.500	2.208	.9042	.9014	.0702	4.45	.9802	.9973
	40.01	4.006	1.506	.9227	.9222	.0284	1.76	.9653	.9747
	40.02	3.203	1.508	.9160	.9153	.0350	2.19	.9629	.9750
	40.03	2.504	1.505	.9085	.9075	.0435	2.75	.9604	.9748
	40.04	1.503	1.503	.8926	.8902	.0651	4.18	.9763	.9750
124	50.01	3.998	3.014	.9188	.9176	.0454	2.84	.9624	.9889
	50.02	3.197	3.010	.9077	.9063	.0522	3.29	.9603	.9895
	50.03	2.503	3.009	.9034	.9013	.0619	3.93	.9578	.9899
	50.04	1.502	3.011	.9016	.8976	.0857	5.45	.9725	.9900
	51.01	4.001	2.212	.9172	.9166	.0334	2.08	.9631	.9868
	51.02	3.196	2.204	.9072	.9064	.0383	2.42	.9612	.9872

Tabulation Of Nozzle Performance Data
Dual Flow Tests (continued)

Config.	Data Point	NPR_p	NPR_s	C_{fgr}	C_{fgx}	C_{fgy}	α degree	C_{dp}	C_{ds}
124	51.03	2.494	2.204	.9003	.8990	.0483	3.07	.9586	.9876
	51.04	1.498	2.209	.8827	.8793	.0771	5.01	.9739	.9881
	52.01	4.012	1.507	.9296	.9294	.0177	1.09	.9628	.9677
	52.02	3.212	1.506	.9242	.9239	.0224	1.39	.9609	.9676
	52.03	2.500	1.505	.9133	.9128	.0304	1.91	.9583	.9678
	52.04	1.501	1.505	.8797	.8779	.0568	3.70	.9689	.9682
224	54.01	4.006	3.025	.9149	.9139	.0440	2.76	.9627	.9887
	54.02	3.208	3.013	.9031	.9017	.0501	3.18	.9605	.9893
	54.03	2.510	3.024	.8964	.8945	.0589	3.77	.9577	.9897
	54.04	1.505	3.019	.8968	.8928	.0843	5.40	.9718	.9897
	55.01	4.013	2.213	.9235	.9130	.0325	2.04	.9627	.9877
	55.02	3.214	2.213	.9024	.9017	.0369	2.35	.9609	.9876
	55.03	2.509	2.215	.8940	.8928	.0453	2.91	.9583	.9877
	55.04	1.504	2.211	.8771	.8738	.0756	4.94	.9723	.9882
	57.01	3.963	1.500	.9256	.9254	.0175	1.09	.9630	.9676
	57.02	3.169	1.499	.9204	.9202	.0217	1.35	.9609	.9677
	57.03	2.481	1.499	.9092	.9088	.0295	1.86	.9584	.9678
	57.04	1.494	1.500	.8731	.8713	.0565	3.71	.9695	.9683
324	58.01	4.000	3.010	.9163	.9149	.0506	3.16	.9628	.9892
	58.02	3.201	3.011	.9046	.9027	.0588	3.72	.9607	.9895
	58.03	2.506	3.011	.8985	.8958	.0701	4.47	.9582	.9894
	58.04	1.514	3.013	.8975	.8923	.0965	6.18	.9729	.9901
	59.01	4.013	2.209	.9145	.9137	.0371	2.33	.9623	.9875
	59.02	3.210	2.214	.9039	.9029	.0432	2.74	.9607	.9877
	59.03	2.508	2.207	.8962	.8946	.0531	3.40	.9581	.9877
	59.04	1.511	2.208	.8775	.8734	.0843	5.51	.9719	.9881
	60.01	4.011	1.505	.9263	.9261	.0198	1.23	.9622	.9670
	60.02	3.216	1.504	.9210	.9207	.0242	1.51	.9606	.9673
	60.03	2.511	1.502	.9105	.9099	.0330	2.08	.9578	.9676
	60.04	1.514	1.503	.8750	.8728	.0620	4.06	.9684	.9680

REFERENCES

1. Wagenknecht, and C. D. Bediako, E. D., "Aerodynamic Performance Investigation Of Advanced Mechanical Suppressor And Ejector Nozzle Concept For Jet Noise Reduction," NASA CR–174860, Feb. 1985.

2. Schloemer, J. J., "Thrust Performance Of An Isolated 32–Chute Suppressor Nozzle With And Without And Ejector At Mach Number 0 and 0.36," GEAE TM 75–77, Feb. 1975.

3. Harrington, D. E., Schloemer, J. J., and Skebe, S. A., "Thrust Performance Of Isolated 36–Chute Suppressor Plug Nozzle With And Without Ejector At Mach Numbers From 0 To 0.45," NASA TM X–3298, Oct. 1975.

4. Mikkelsen, K. L., "Model Tests To Determine Static Performance Of A High Speed Civil Transport Fluid Shield Nozzle," Conducted For GE Aircraft Engines, FluiDyne Engineering Corporation, Report 1911, Dec. 1992.

5. Wagenknecht, and C. D. Bediako, E. D., "Aerodynamic Performance Investigation Of Thermal Acoustic Shield Nozzle," NASA CR–174867, Jan. 1985.

Table I. – Axisymmetric Plug Fluid Shield Nozzle Test Configurations

Configuration	Primary Nozzle Throat Area, A_8 in^2	Shield Flow Area A_{18}, in^2	Shield Wrap Angle, deg	Shield Throat Height, fld ht in	Primary Plug
111	21.990	12.080	220	0.50	15° Solid
211					15° Porous
311					18° Solid
112	21.990	18.375	220	0.75	15° Solid
212					15° Porous
312					18° Solid
113	21.990	24.596	220	1.00	15° Solid
213					15° Porous
313					18° Solid
114	21.990	11.785	180	0.60	15° Solid
214					15° Porous
314					18° Solid

Table II – Plug Static Pressure Locations

15 deg Plug L = 15.163 in		18 deg Plug L = 12.502 in	
Primary X/L	Secondary X/L	Primary X/L	Secondary X/L
.0445	.0445	.0546	.0546
.1082	.1082	.1196	.1196
.1718	.1718	.1844	.1844
.2355	.2355	.2492	.2492
.2990	.2990	.3141	.3141
.3627	.3627	.3790	.3790
.4264	.4264	.4439	.4439
.4899	–	.5088	–
.5536	.5536	.5737	.5737
.6173	–	.6386	–
.6809	.6809	.7035	.7035
.8082	.80082	.8333	.8333

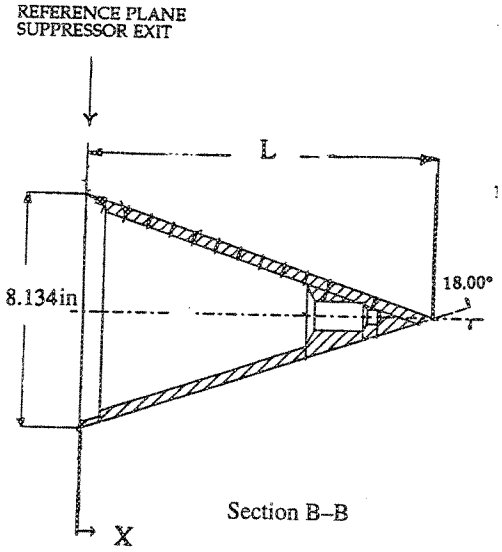

Section B–B

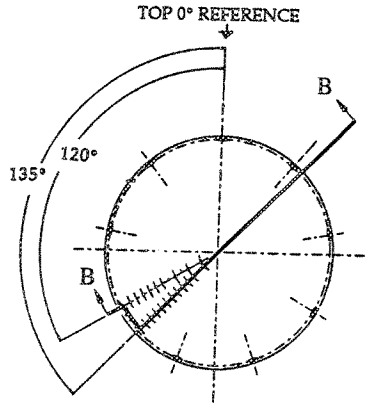

View AFT Looking Forward
(See Figure 8b)

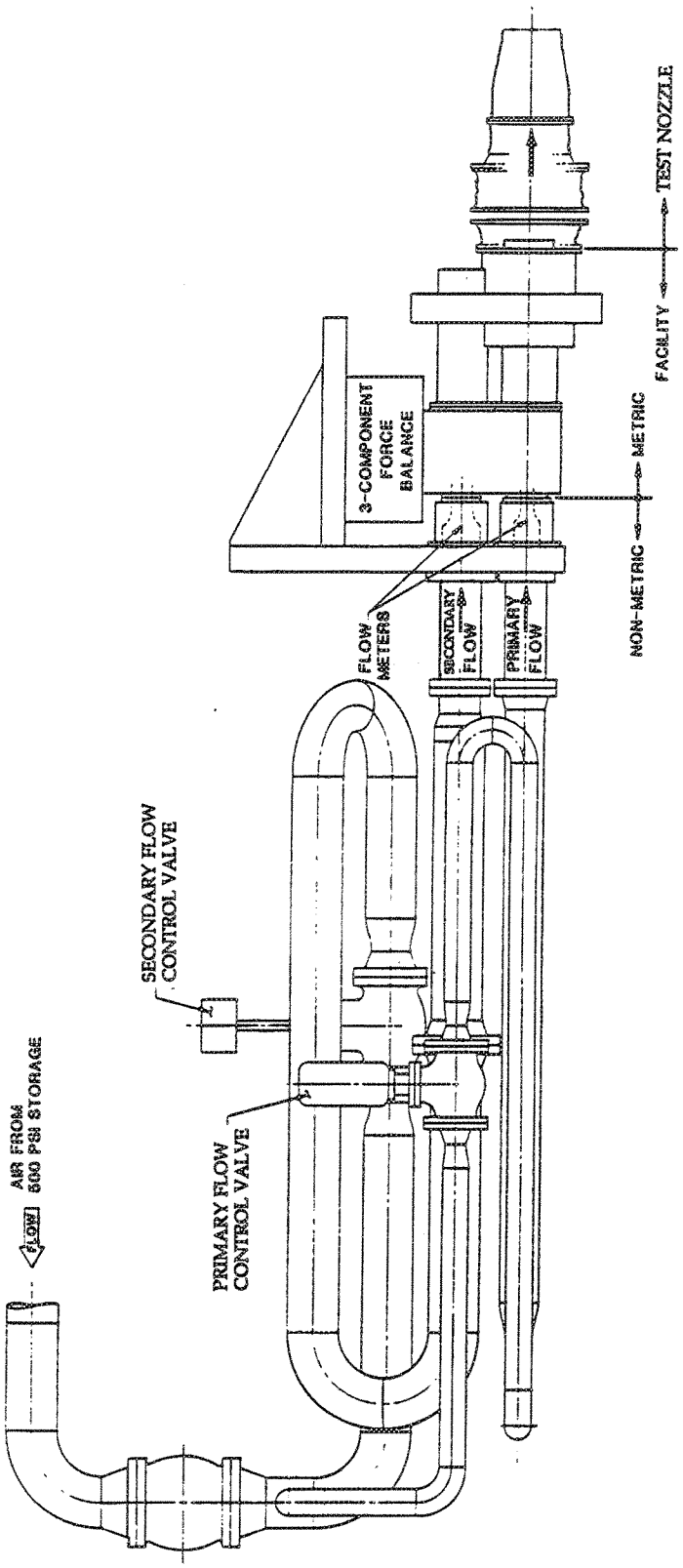

Figure 1. Channel 14 Static Thrust Stand.

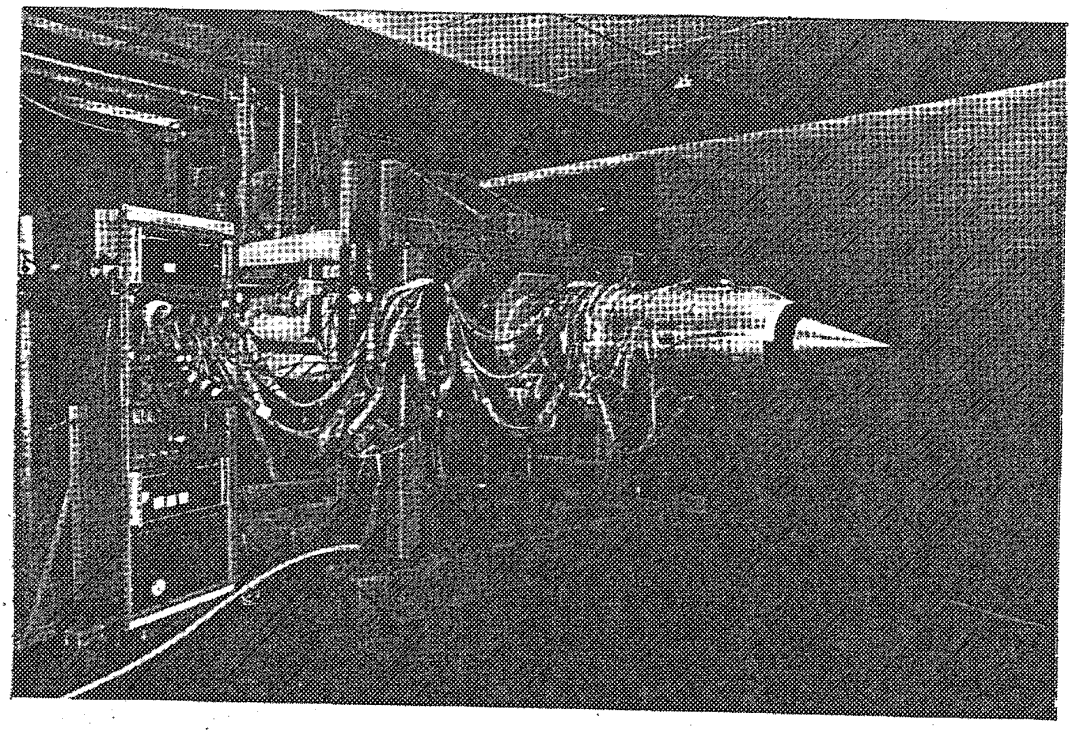

a) Fluid Shield Nozzle

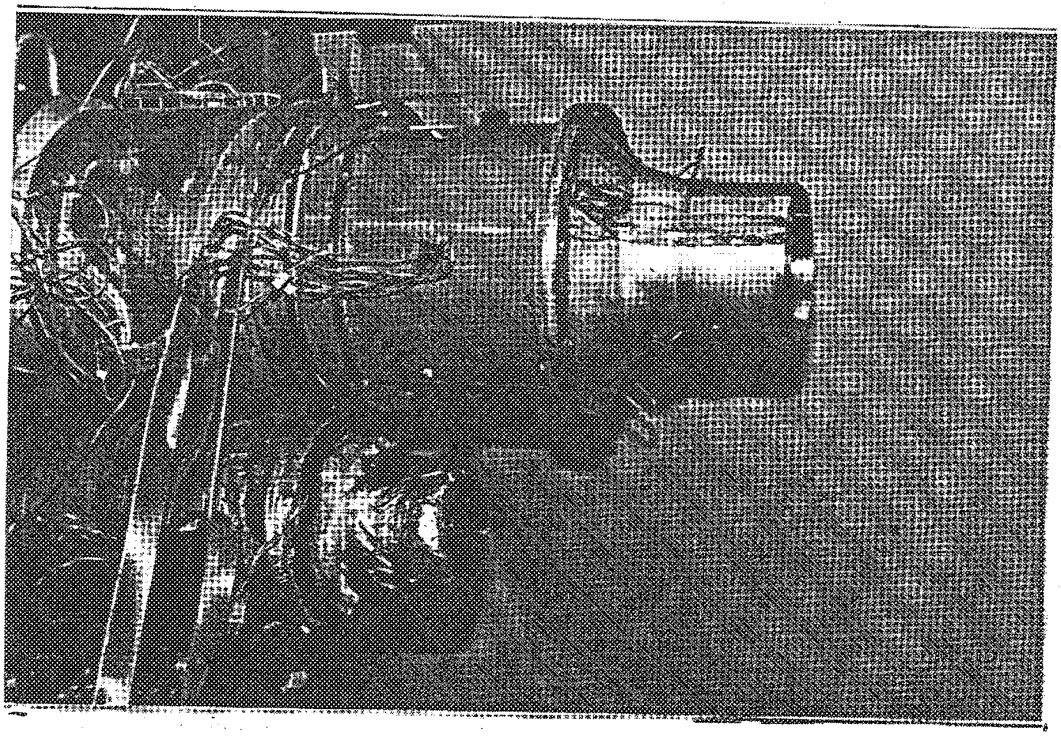

b) ASME Checkout Nozzle

Figure 2. Channel 14 Model Test Setup.

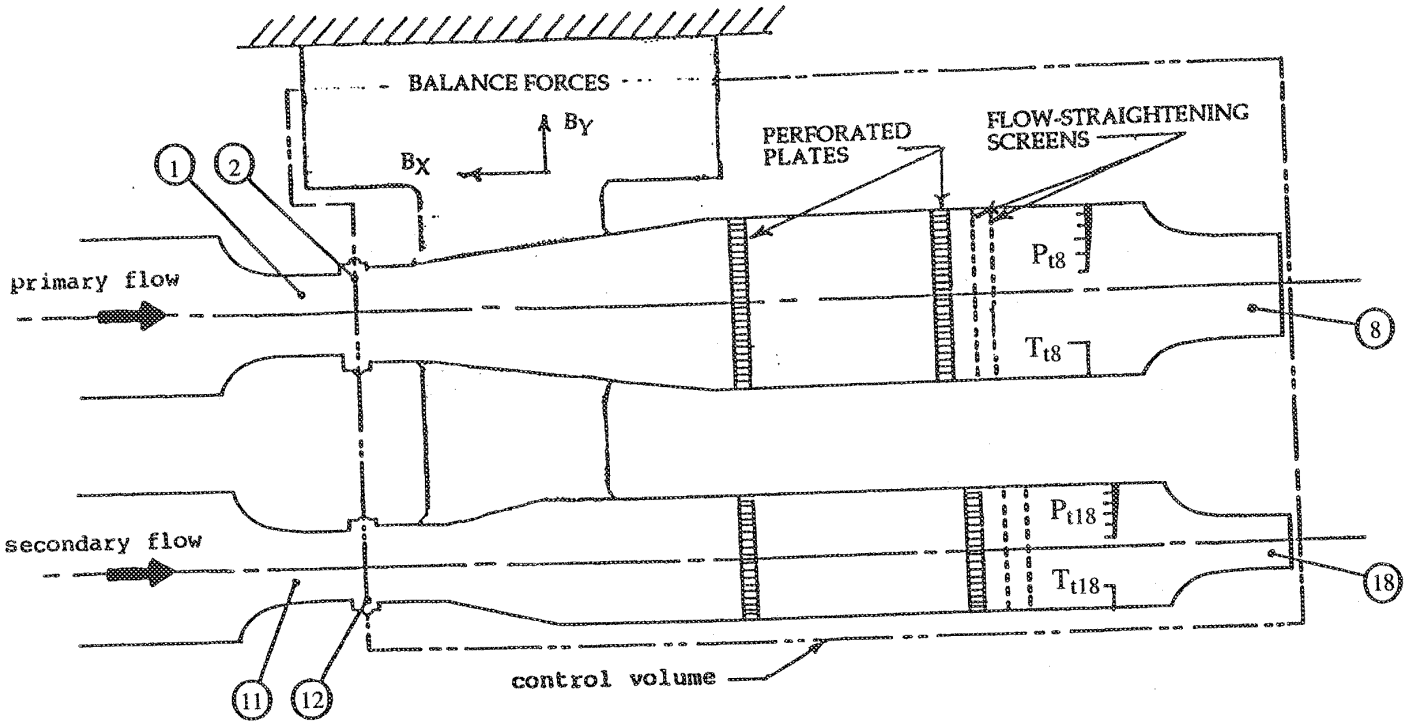

Station	Description
1	ASME meter throat (primary flow)
2	Flexible seal (primary flow)
8	ASME checkout nozzle throat (primary flow)
11	ASME meter throat (secondary flow)
12	Flexible seal (secondary flow)
18	ASME checkout nozzle throat (secondary flow)

Figure 3. ASME Checkout Nozzle Station Notation.

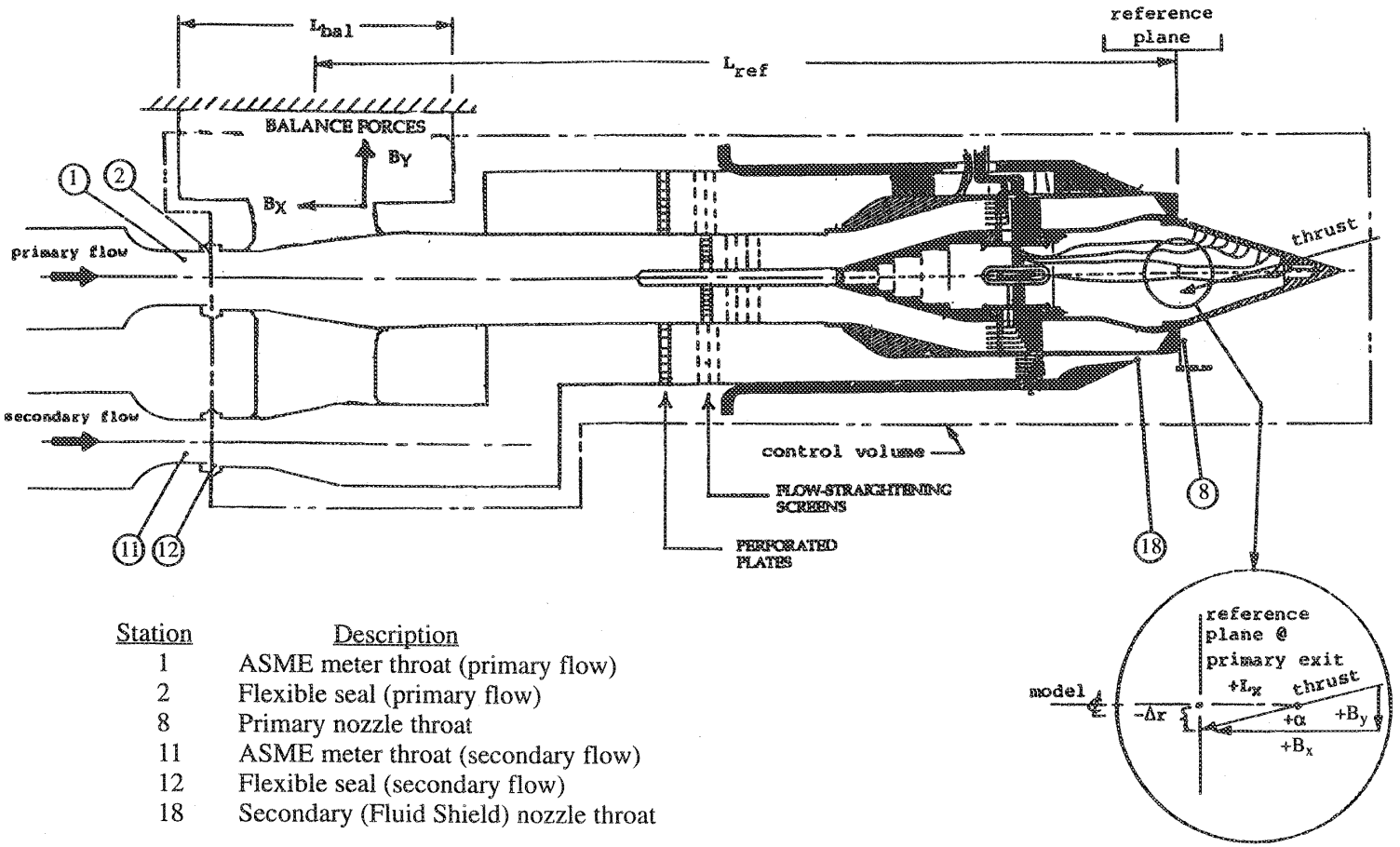

Station	Description
1	ASME meter throat (primary flow)
2	Flexible seal (primary flow)
8	Primary nozzle throat
11	ASME meter throat (secondary flow)
12	Flexible seal (secondary flow)
18	Secondary (Fluid Shield) nozzle throat

Figure 4. Fluid Shield Nozzle Station Notation.

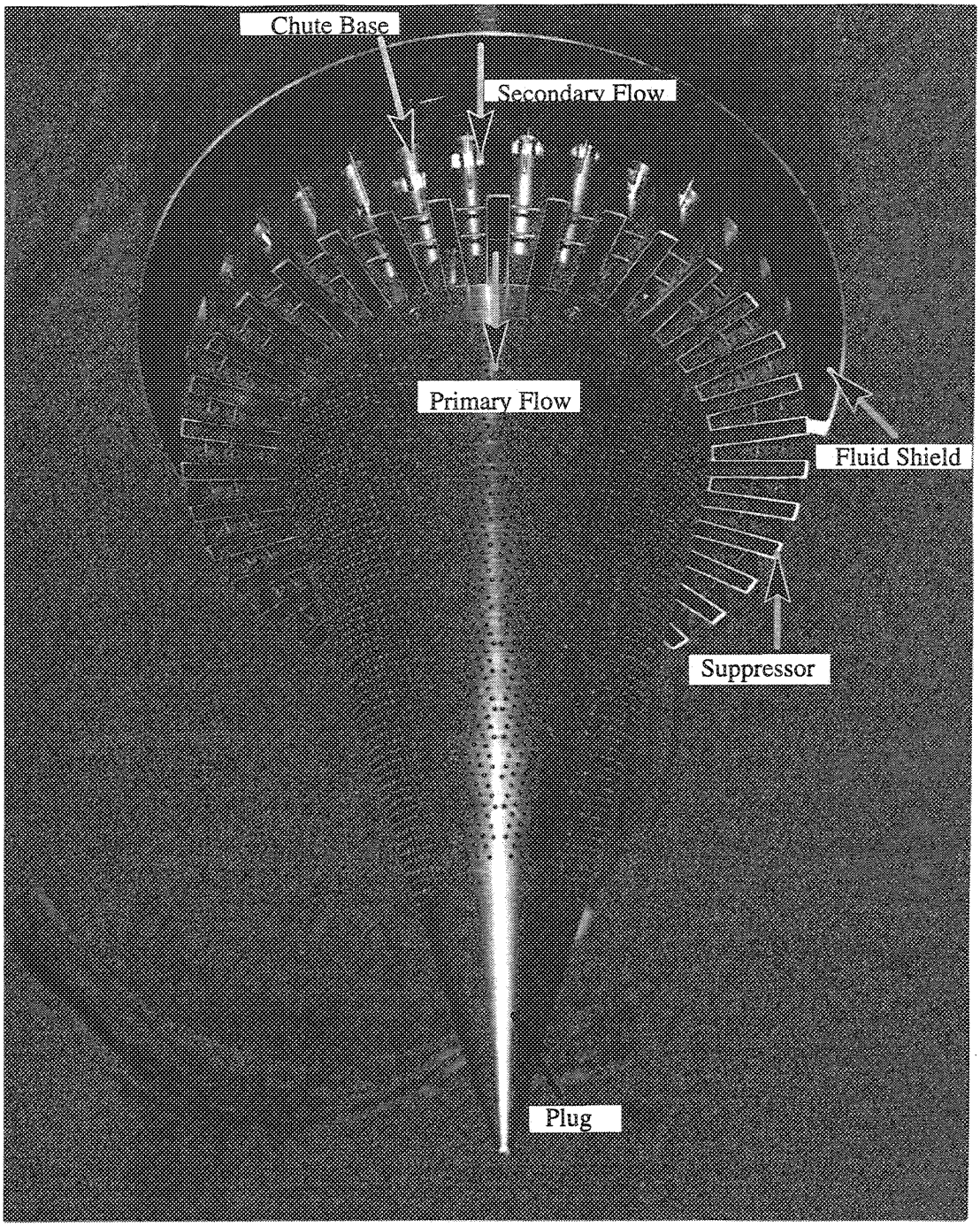

Figure 5. Fluid Shield Nozzle with Porous Plug

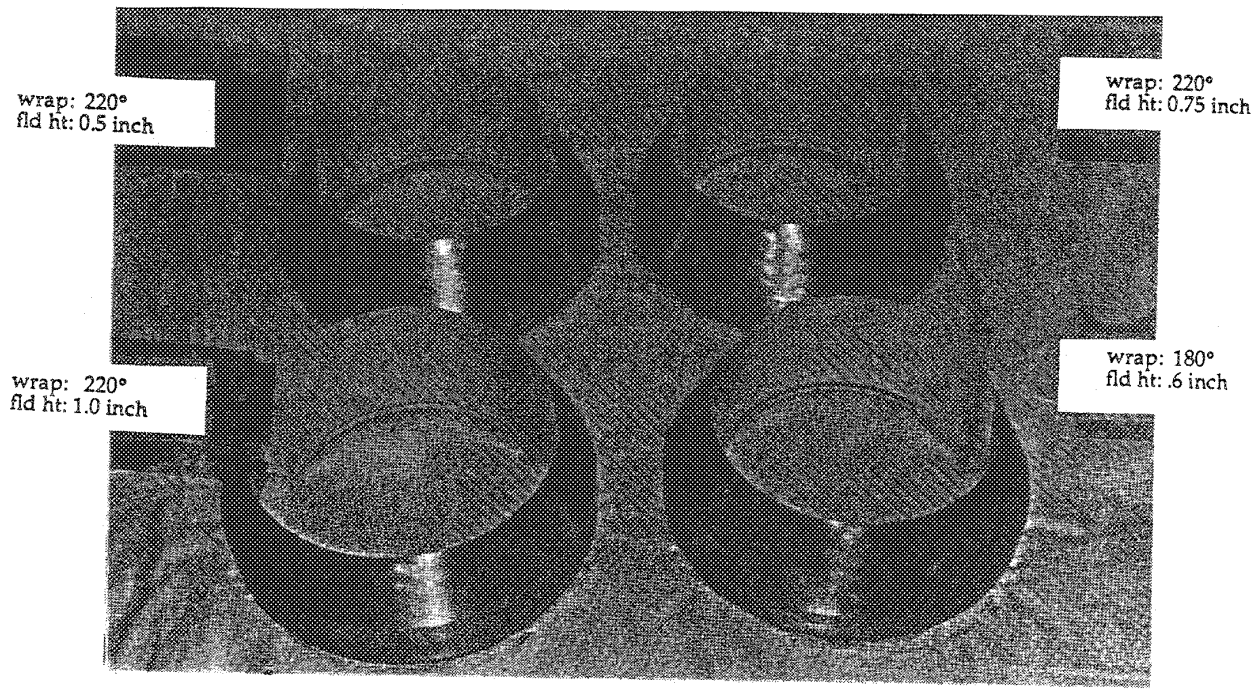

a) Fluid Shield Hardware.

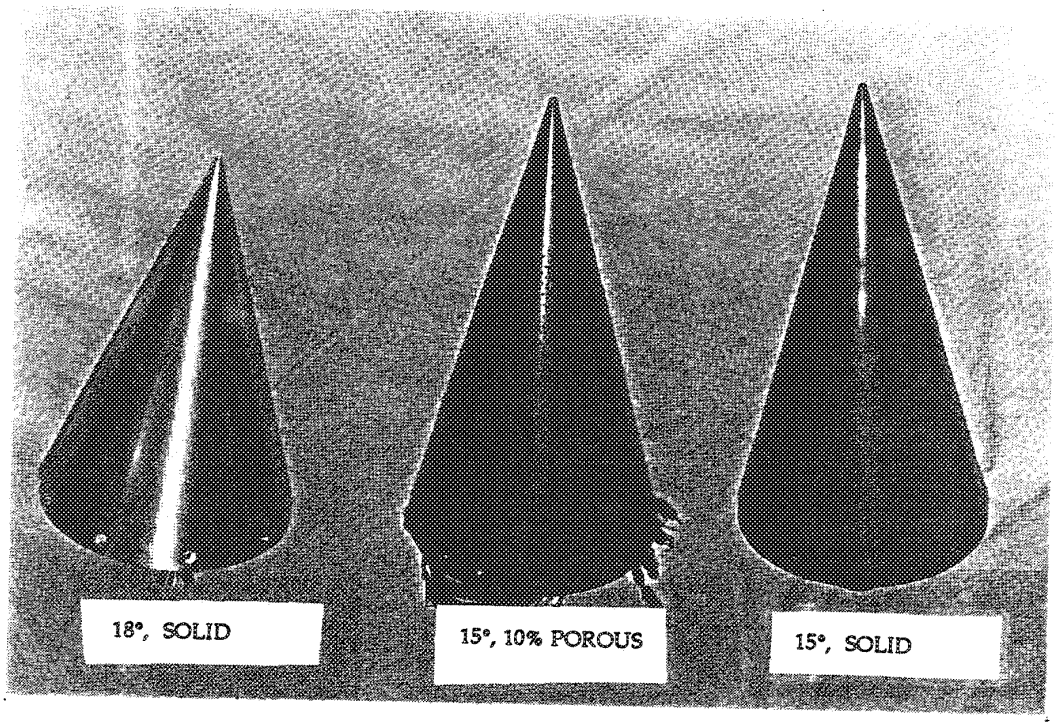

b) Plug Hardware.

Figure 6. Model Hardware.

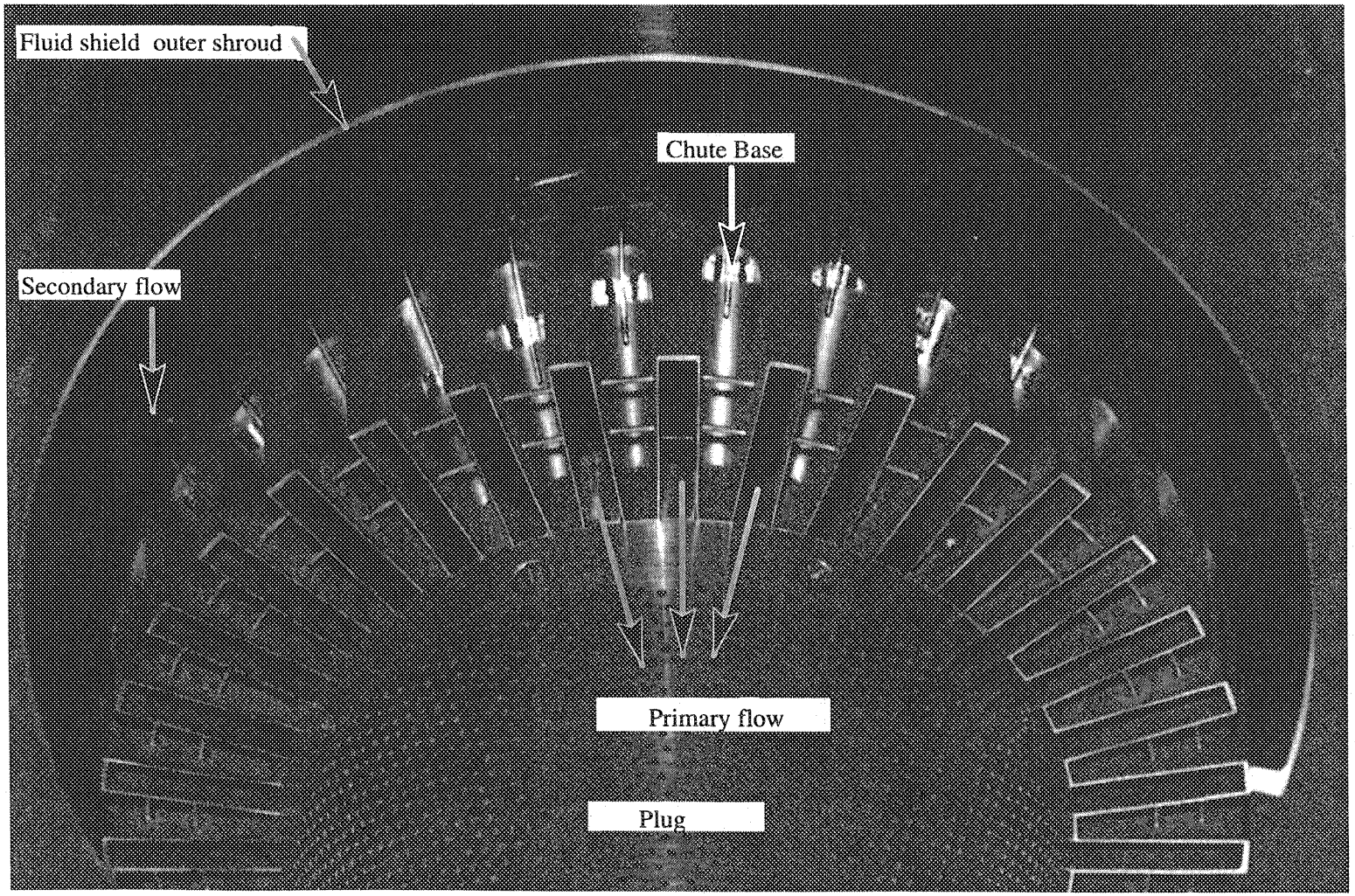

c) View of the supressor chutes and fluid shield

Figure 6. Fluid shield model hardware (concluded).

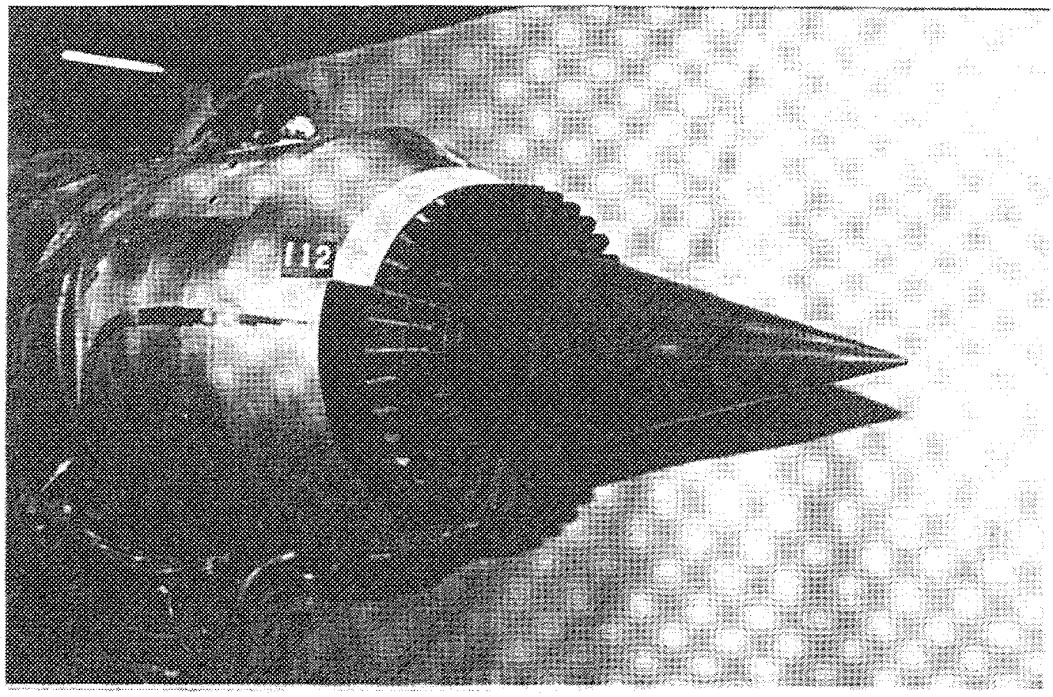

a) Nozzle with 15^0 solid plug, 0.75" – 220^0 fluid shield (configuration 112)

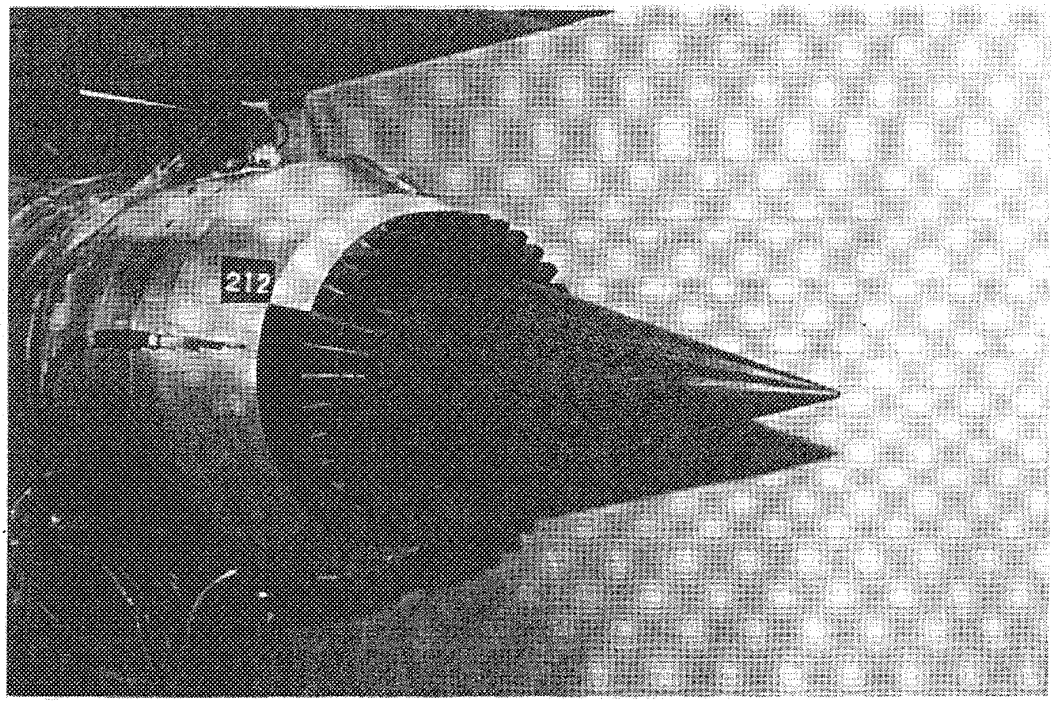

b) Nozzle with 15^0 porous plug, 0.75" – 220^0 fluid shield (configuration 212)

Figure 7. Selected views of fluid shield nozzle test configurations.

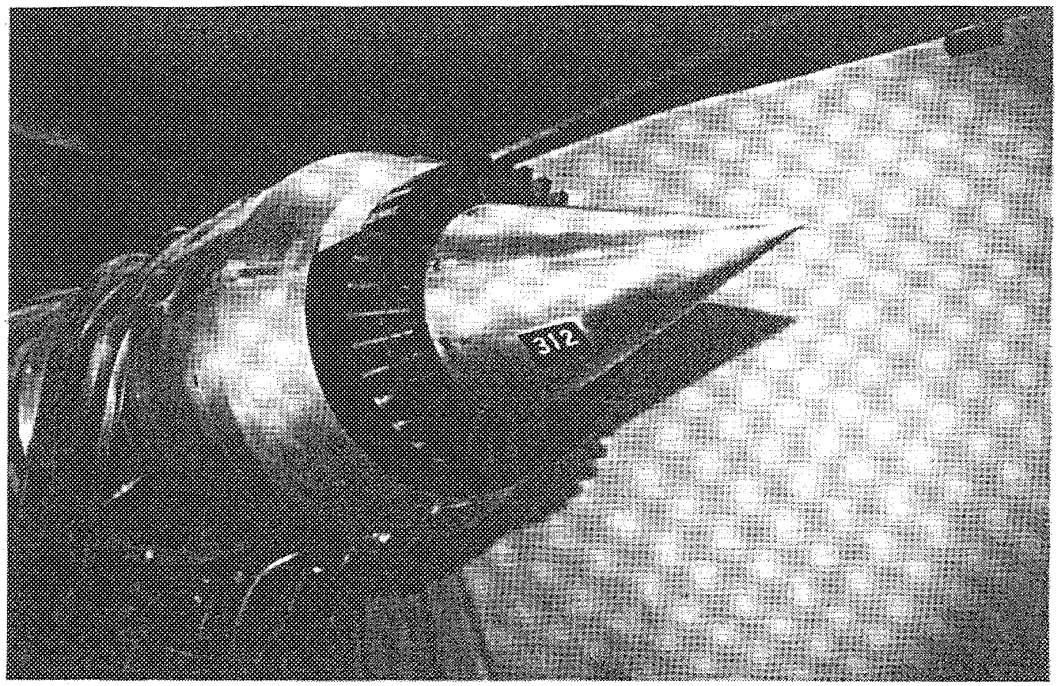

c) Nozzle with 18^0 solid plug, 0.75" – 220^0 fluid shield (configuration 312)

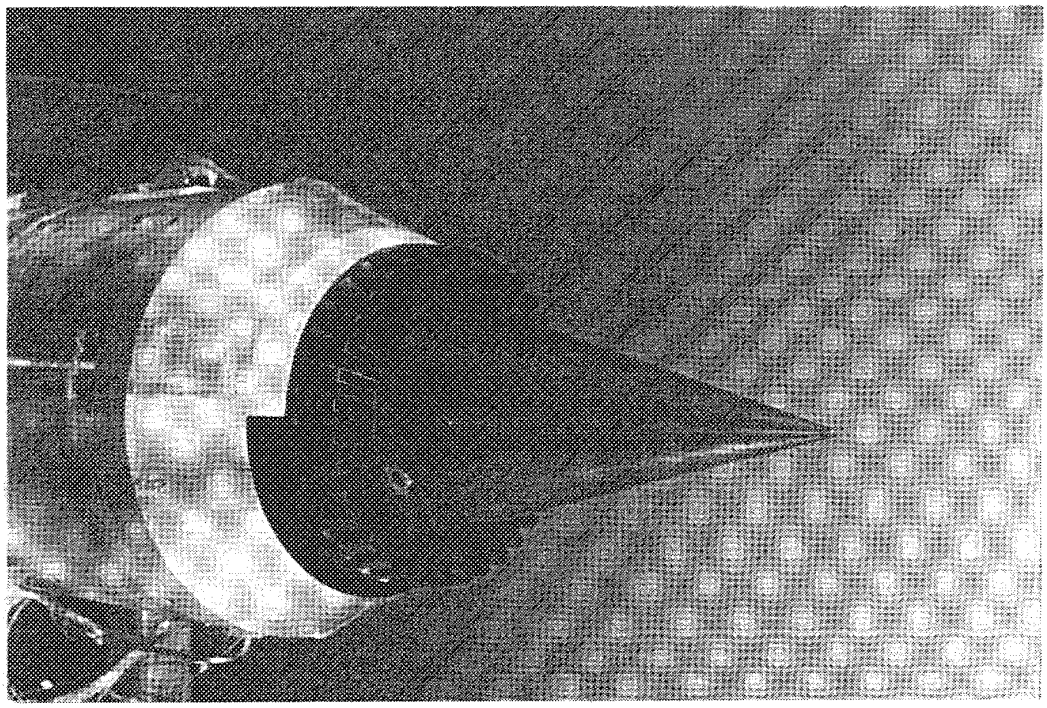

d) Nozzle with 15^0 solid plug, 0.60" – 180^0 fluid shield (configuration 124)

Figure 7. Concluded.

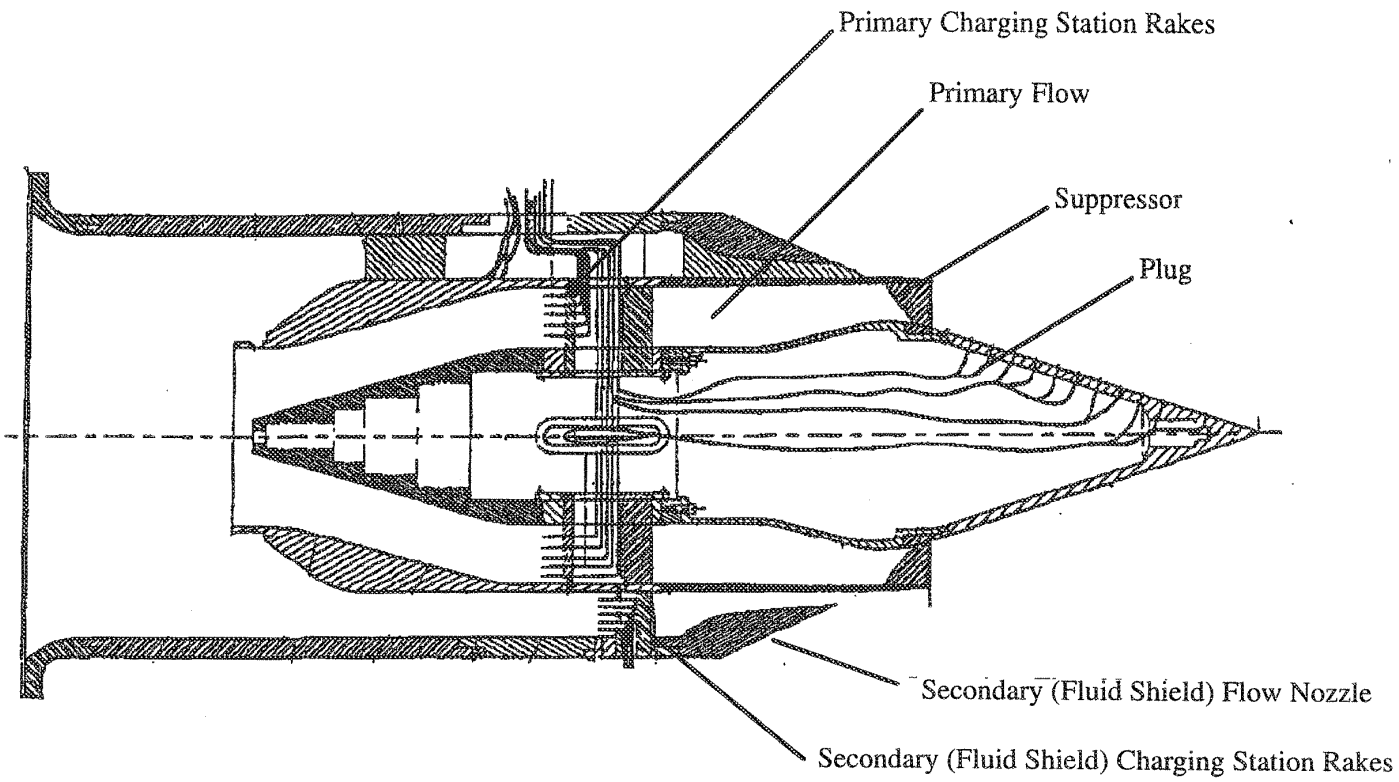

Figure 8a. Fluid shield model cross section showing charging station rakes.

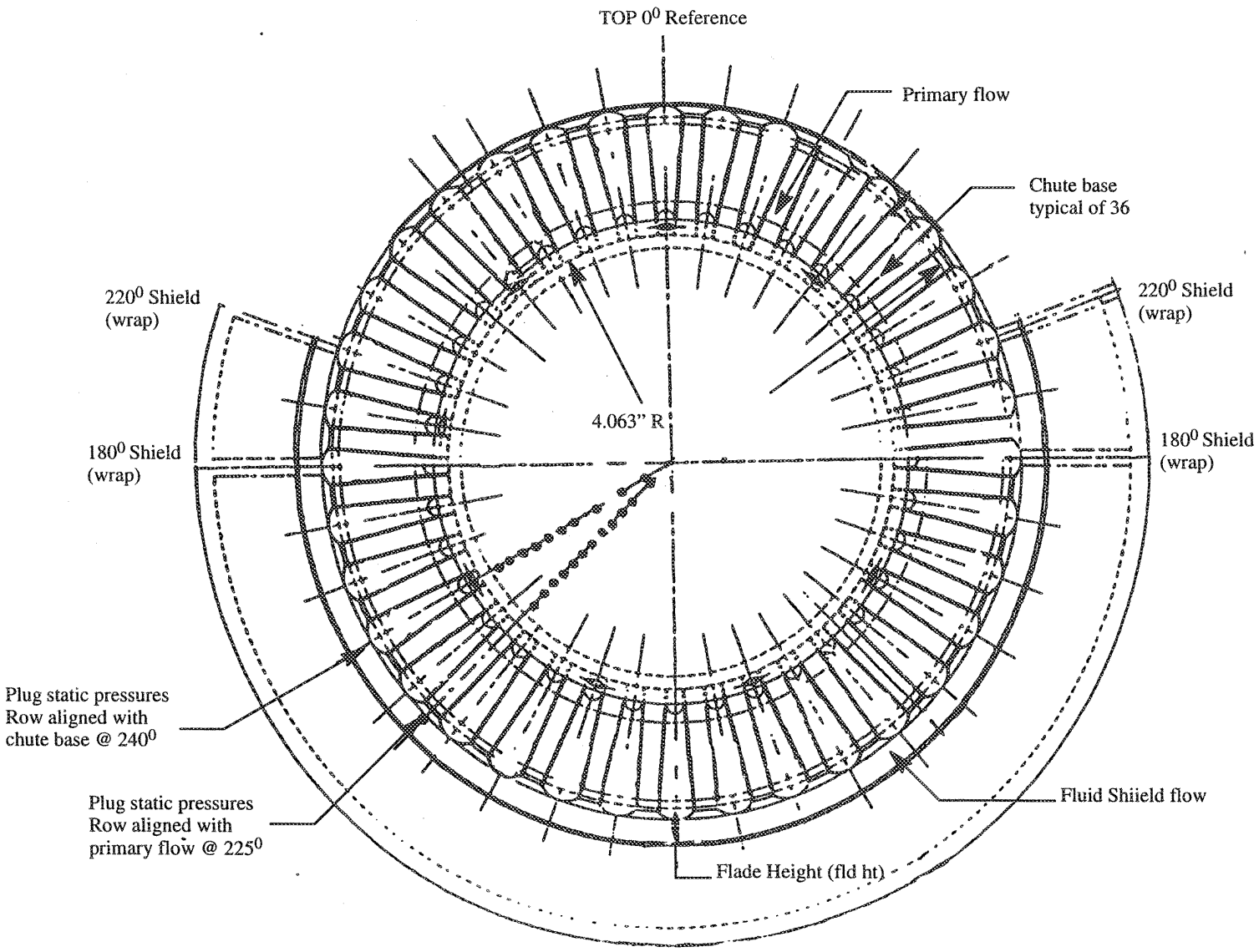

Figure 8b. Fluid shield model view – AFT looking Forward.

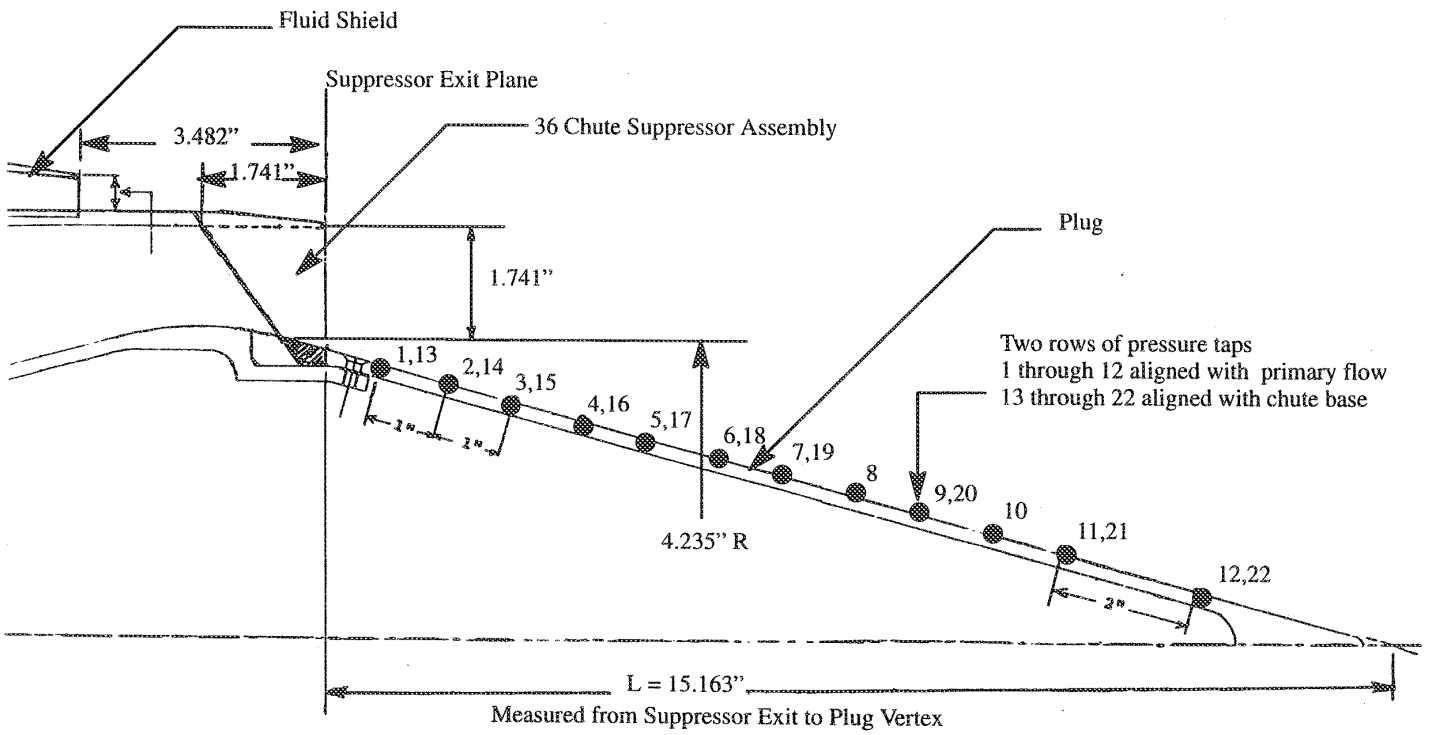

Figure 8c. Fluid Shield Nozzle Plug Static Pressure Instrumentation.

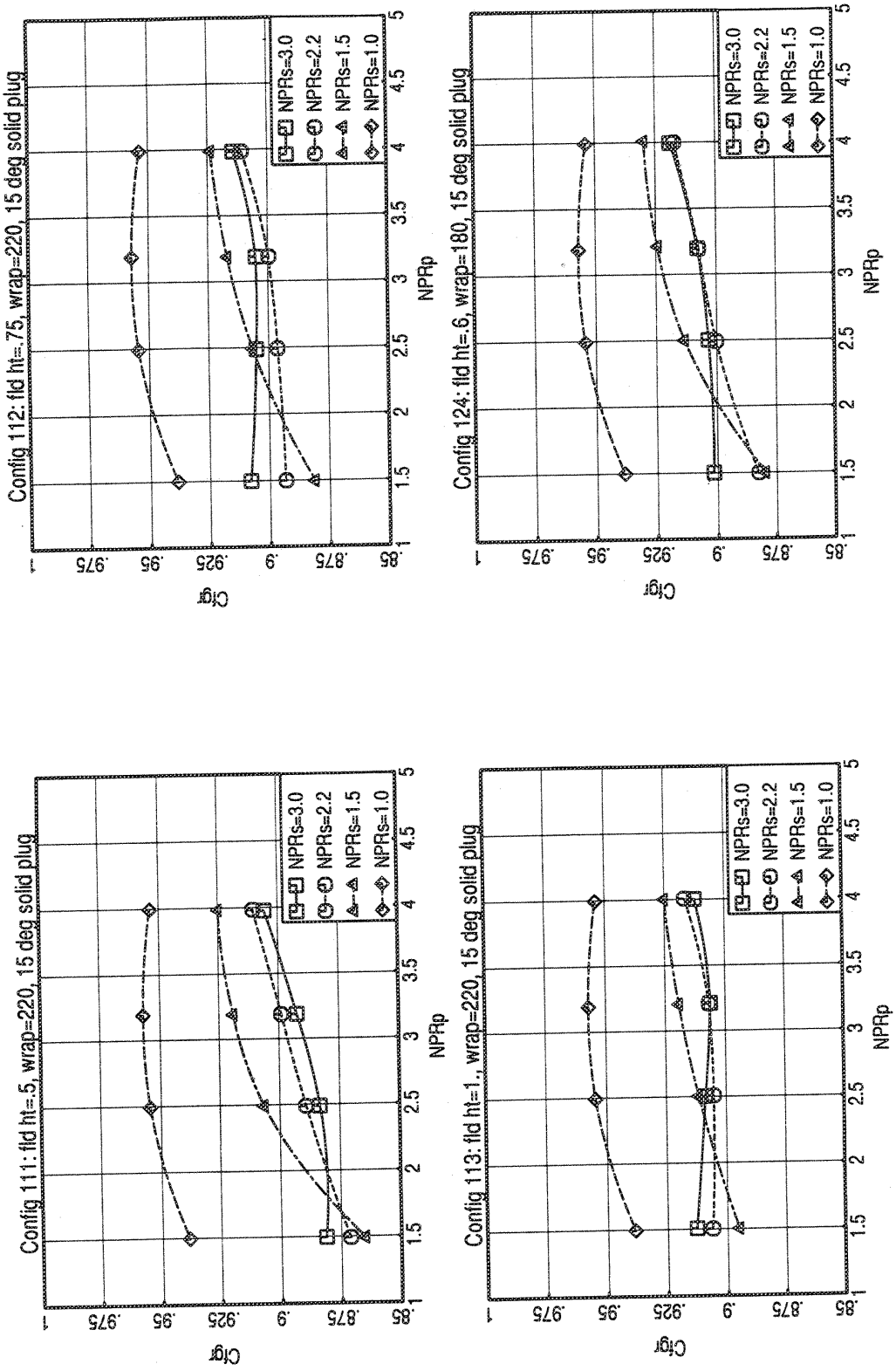

a) 15° Solid Plug Configurations

Figure 9. Comparison Of Static Thrust Coefficients.

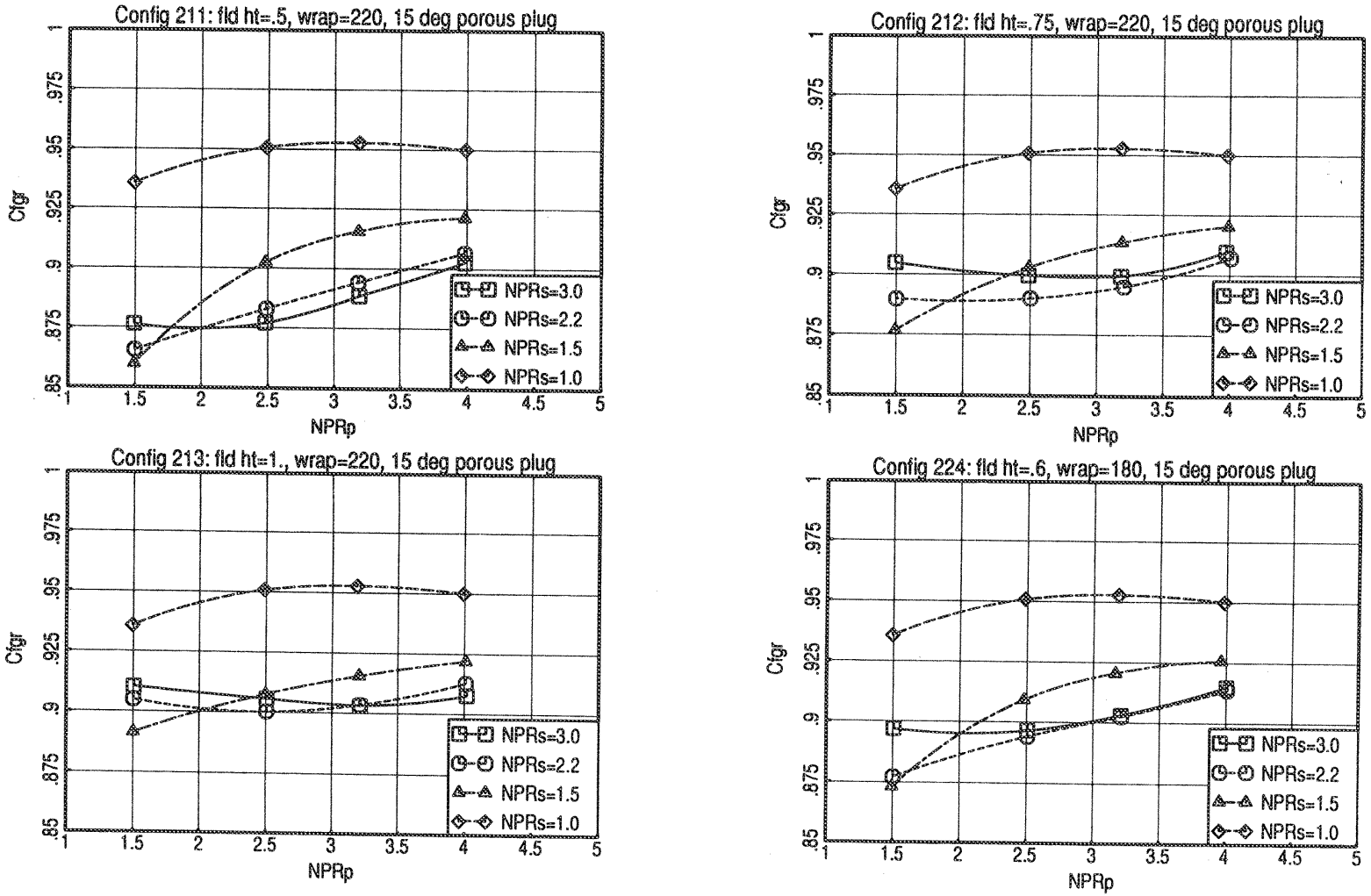

b) 15° Porous Plug Configurations

Figure 9. Continued.

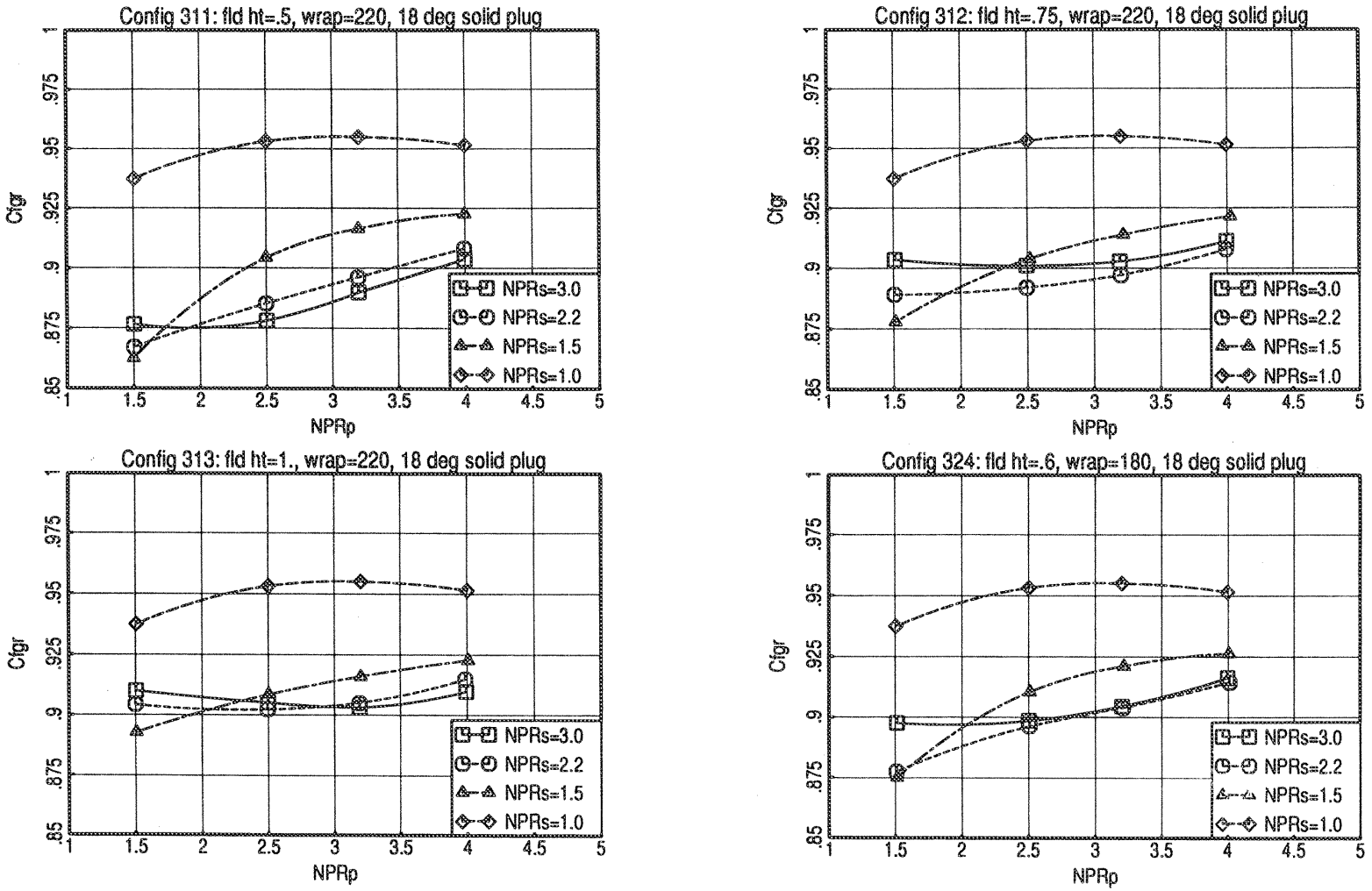

c) 18° Solid Plug Configurations

Figure 9. Concluded.

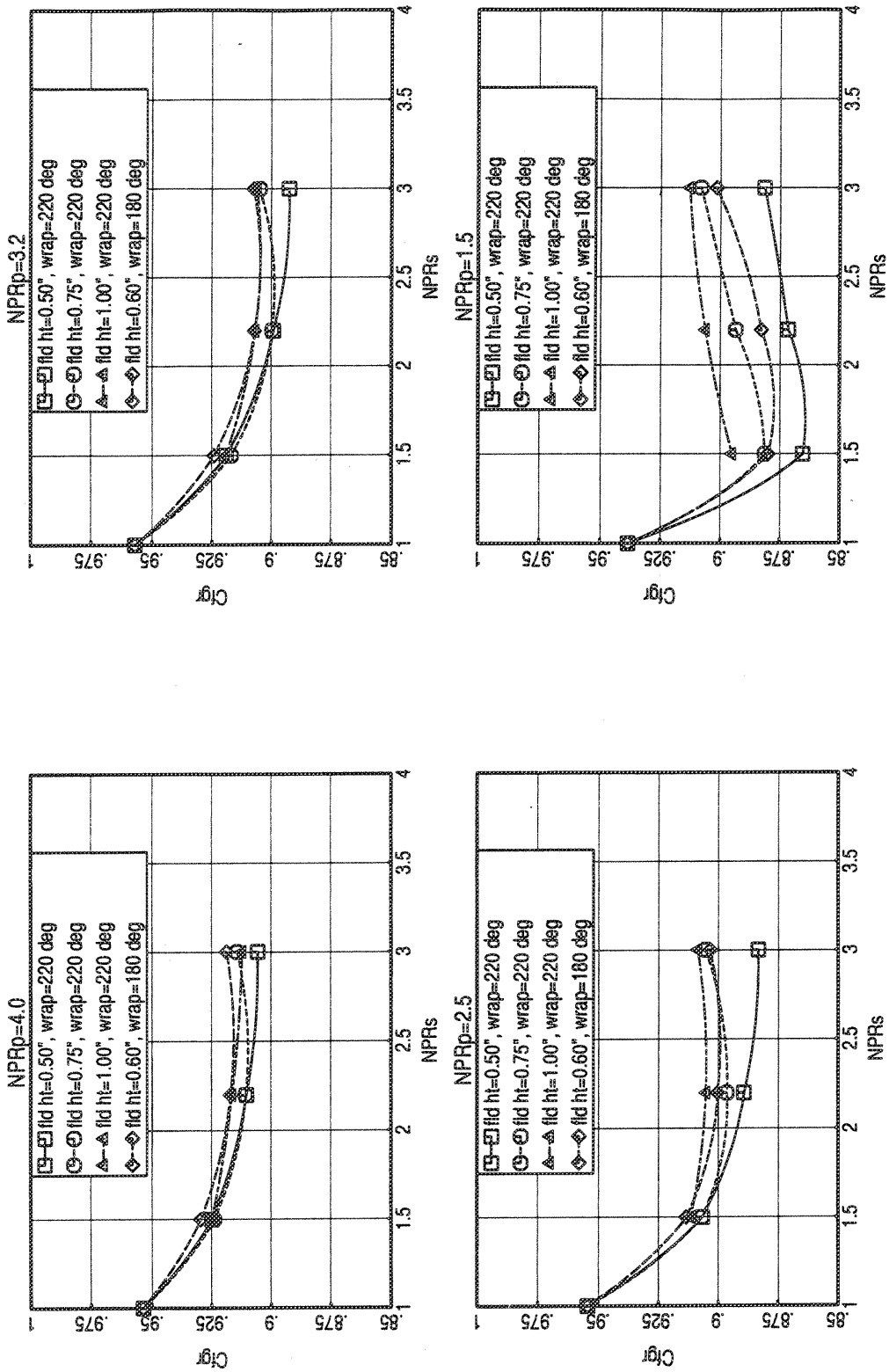

Figure 10. Shield Effect On Nozzle Static Thrust Coefficients, 15° Solid Plug.

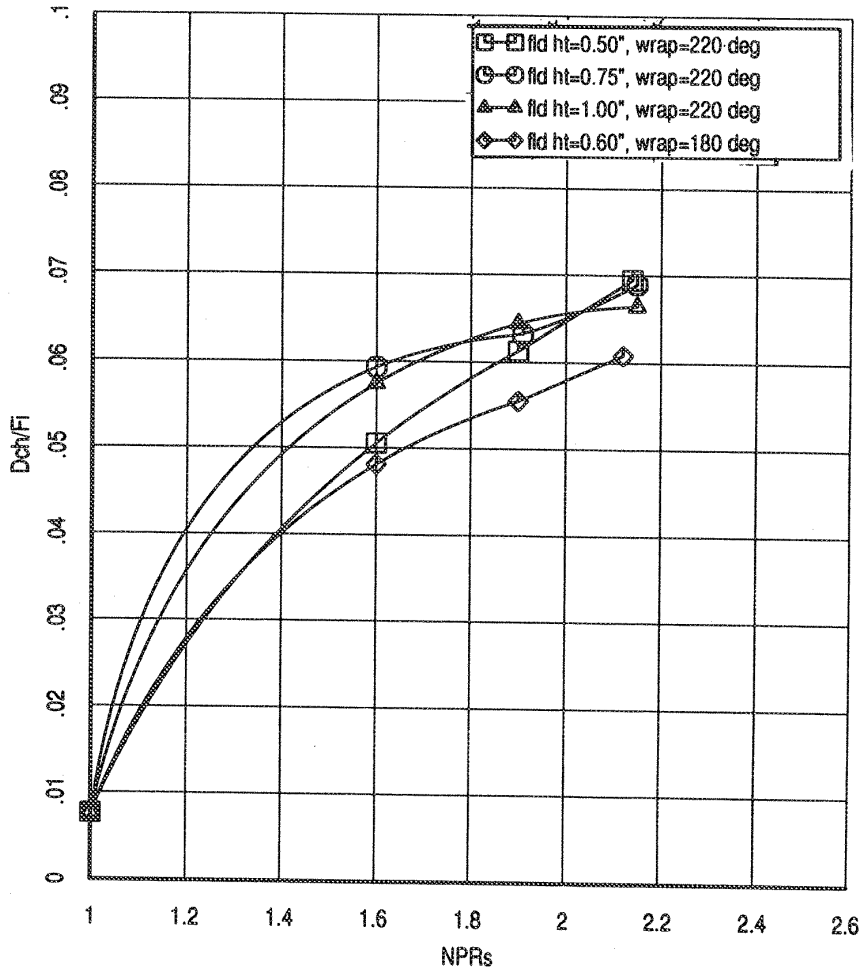

Figure 11. Fluid Shield Nozzle Thrust Loss From Chute–Base Pressure Drag;
NPR_p = 3.2, 15° Porous Plug
(Unpublished Cell41 data from Task Order 9 of Contract NAS3–25951

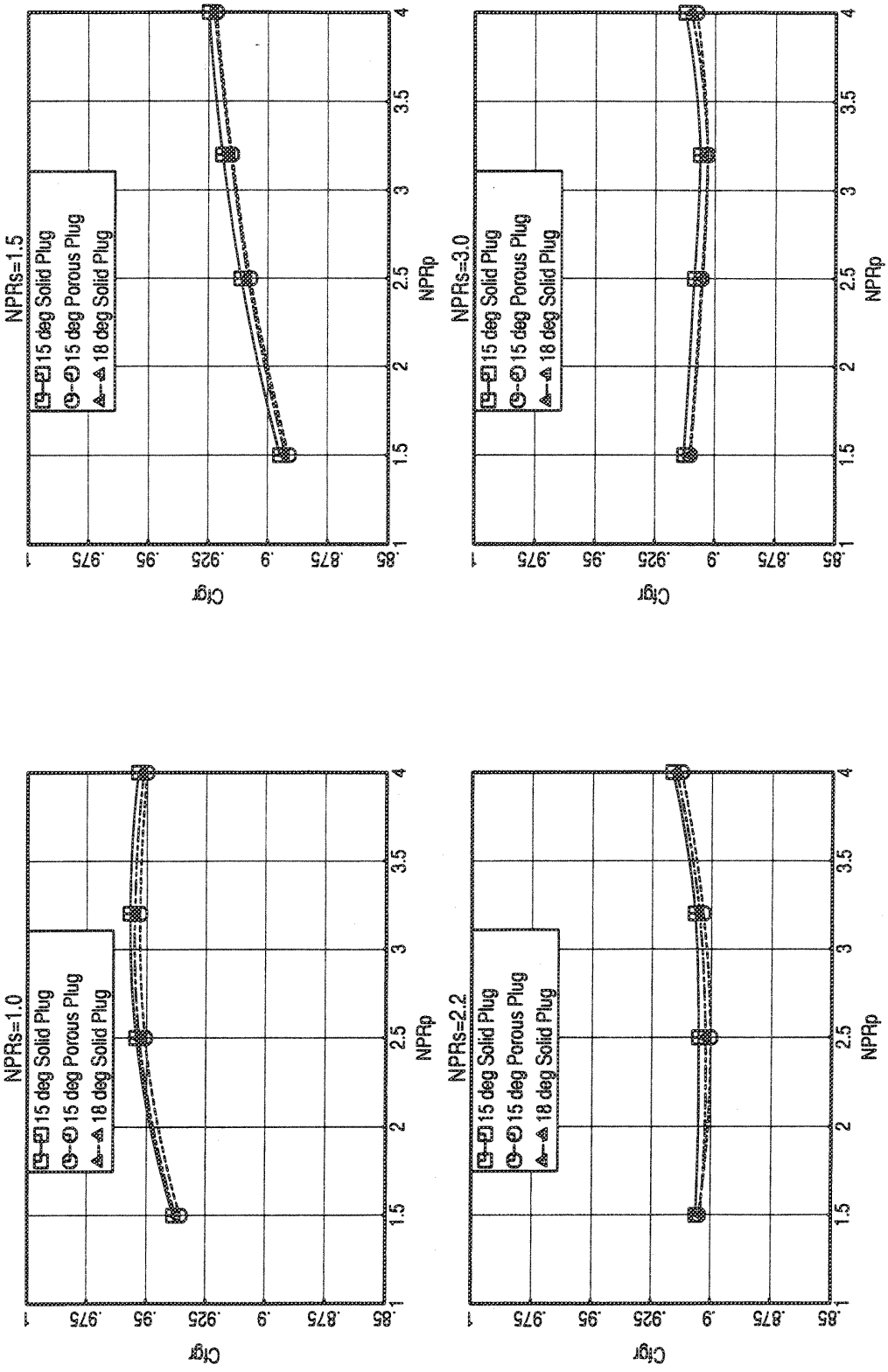

Figure 12. Plug Effect On Nozzle Static Thrust Coefficients.

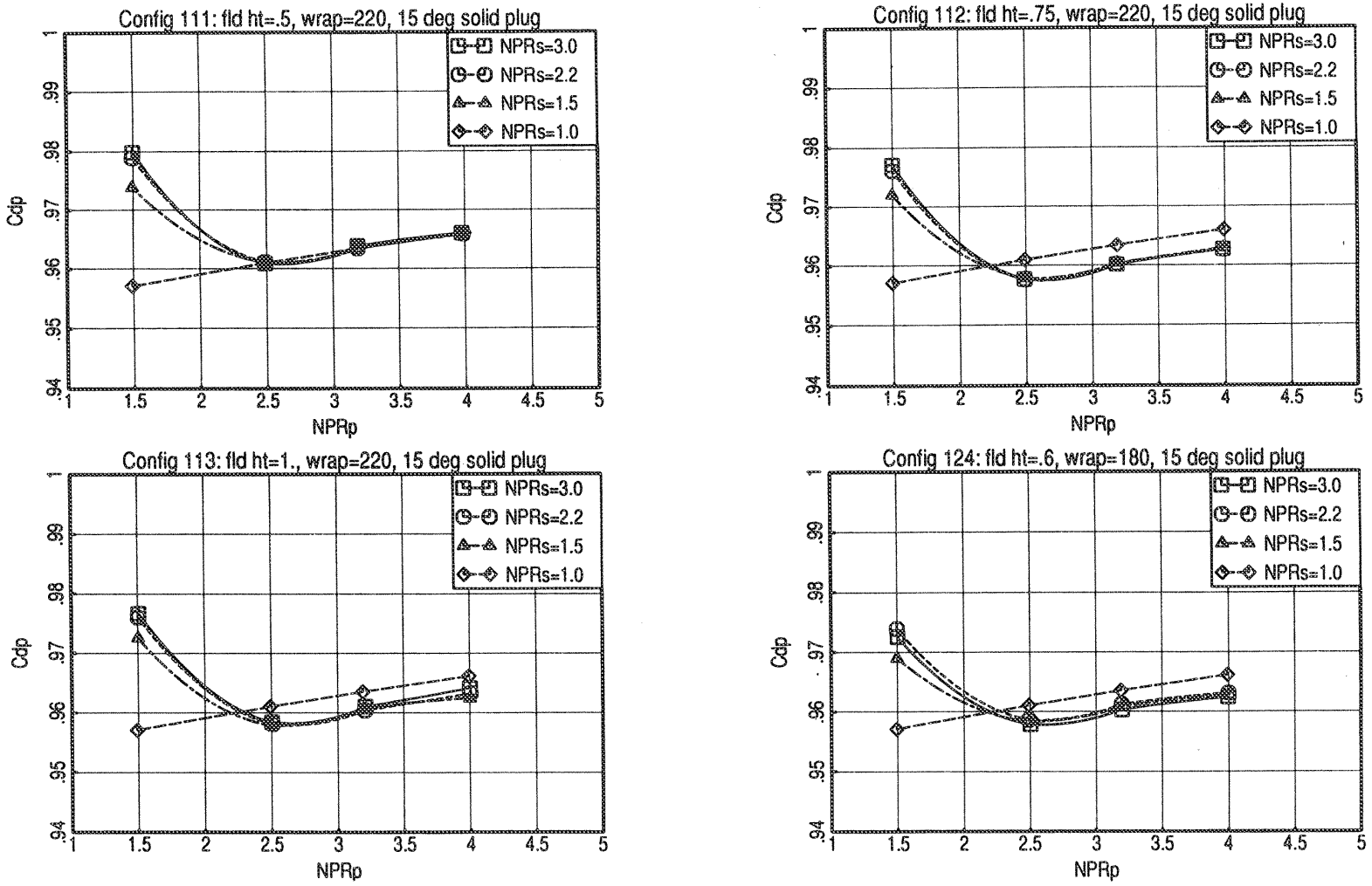

a) 15° Solid Plug Configurations

Figure 13. Comparison Of Primary Nozzle Flow Coefficients.

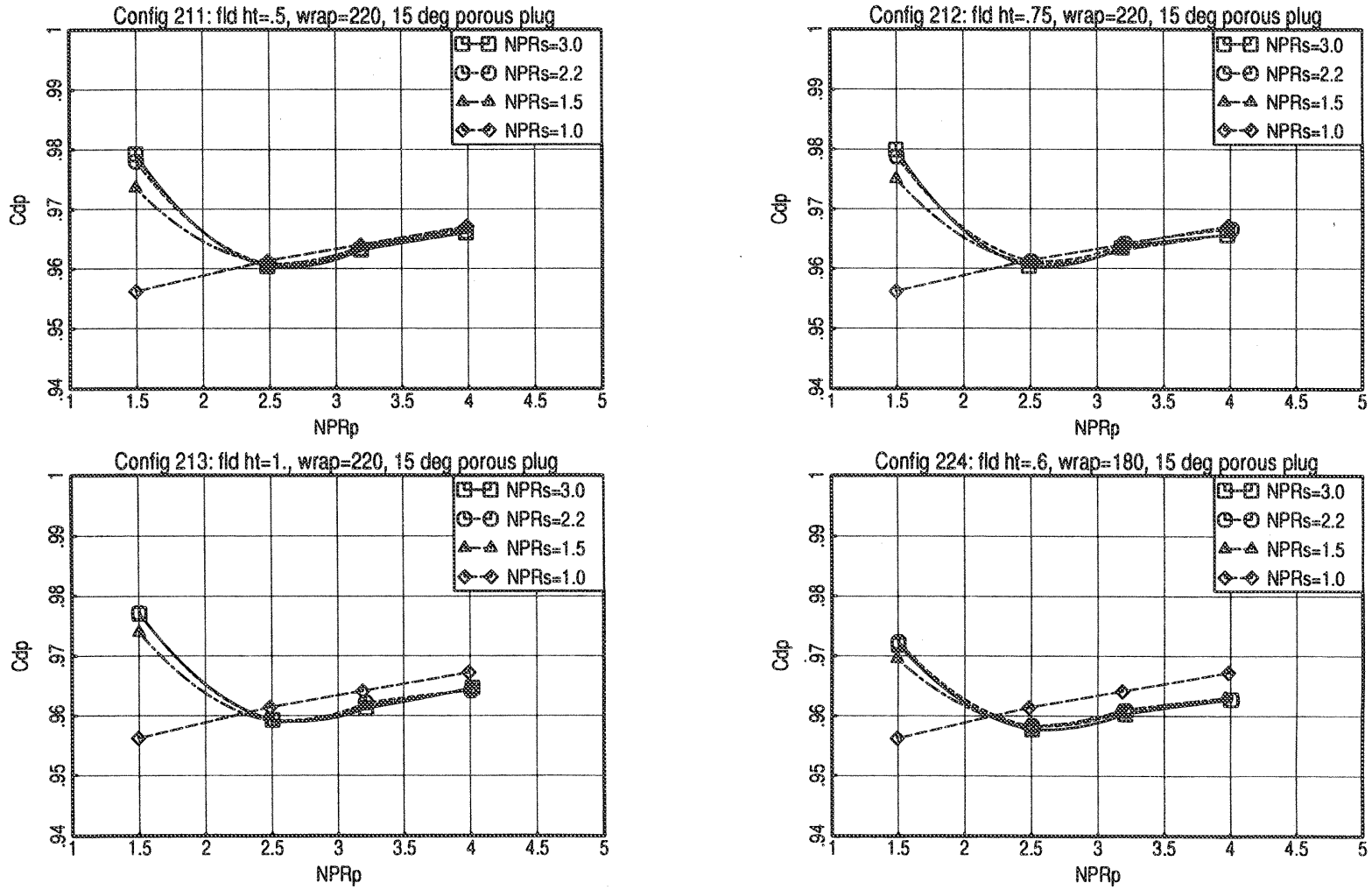

b) 15° Porous Plug Configurations

Figure 13. Continued.

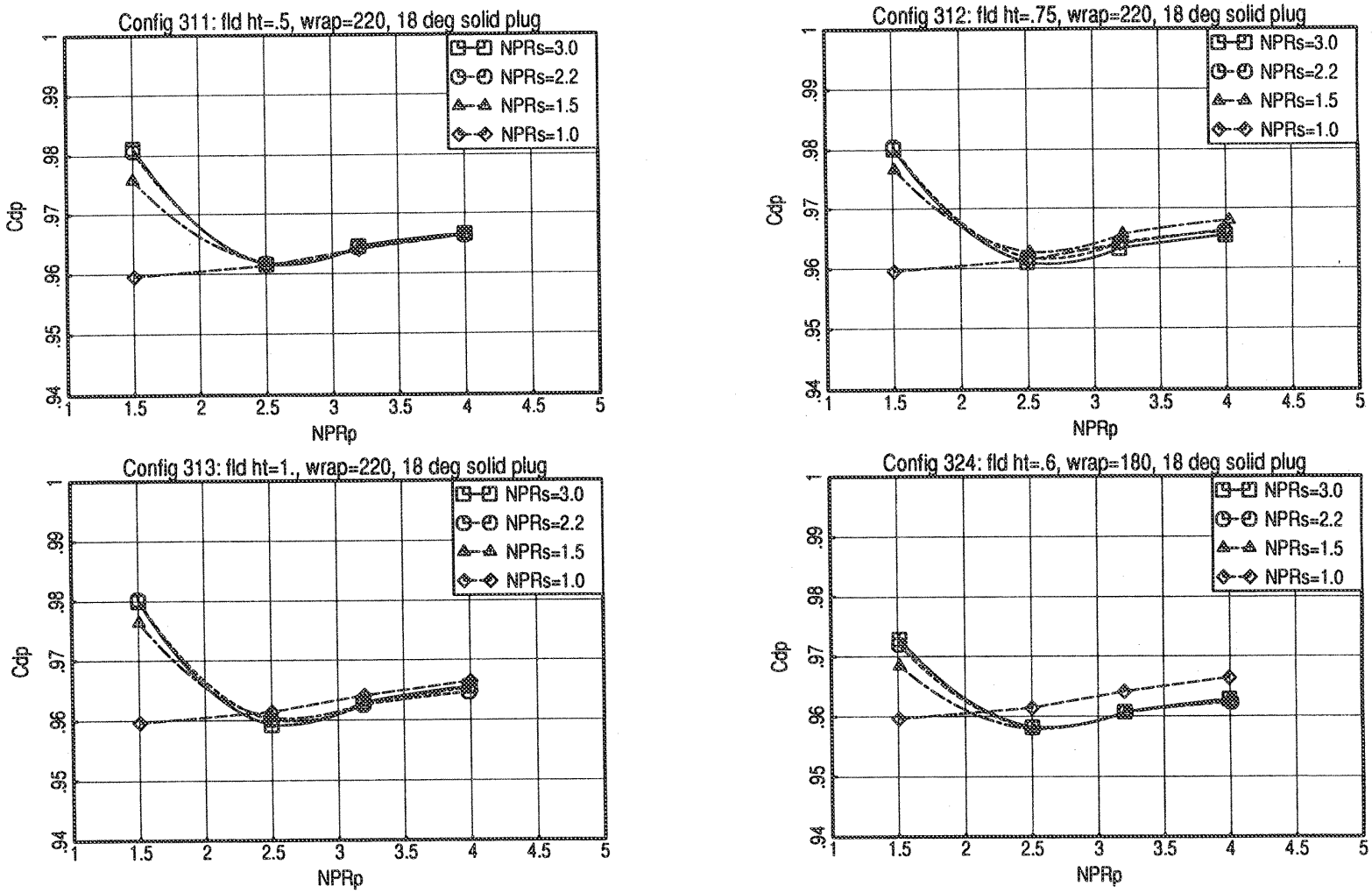

c) 18° Solid Plug Configurations

Figure 13. Concluded.

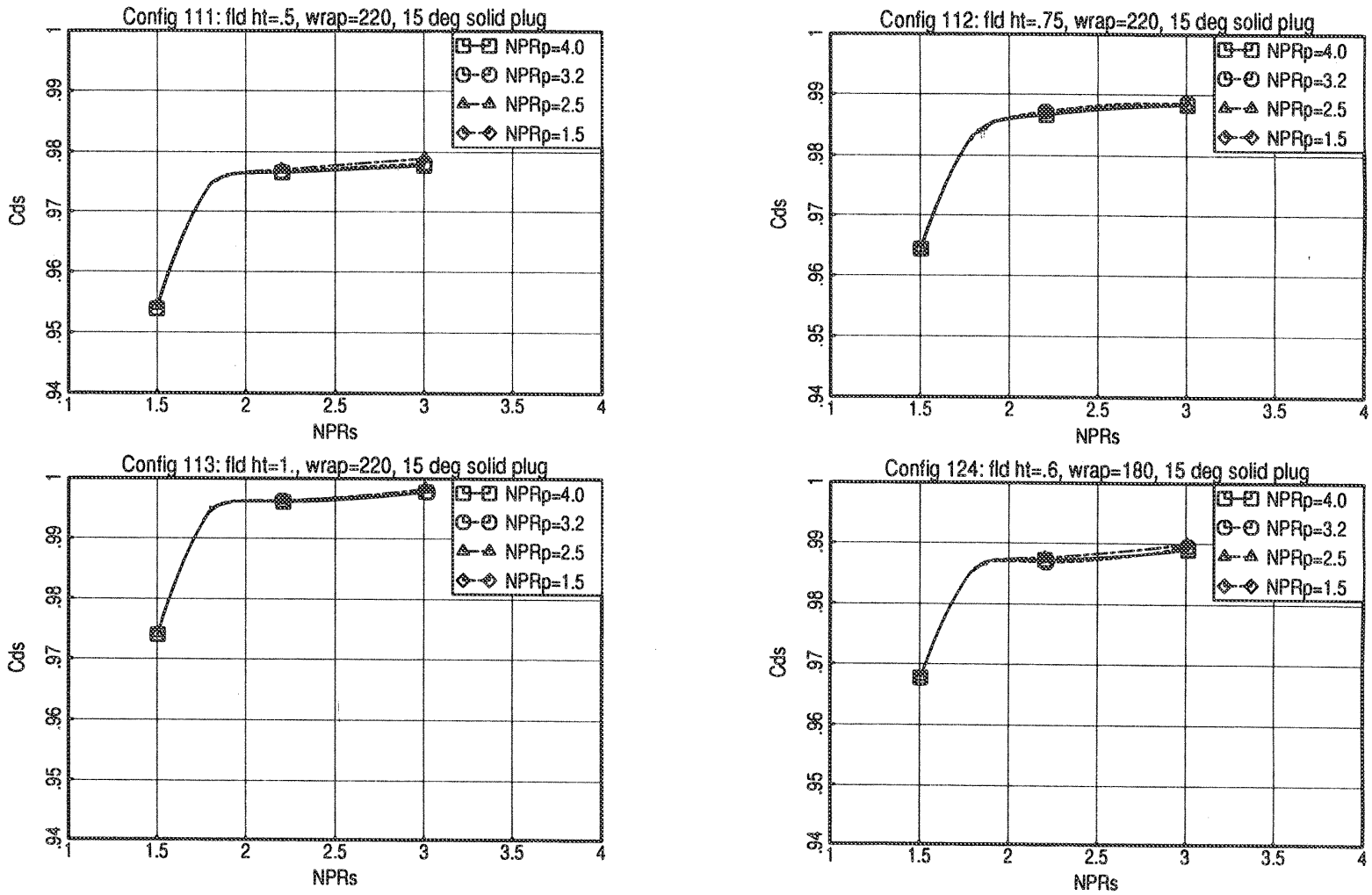

a) 15° Solid Plug Configurations

Figure 14. Comparison Of Secondary (Fluid Shield) Nozzle Coefficients.

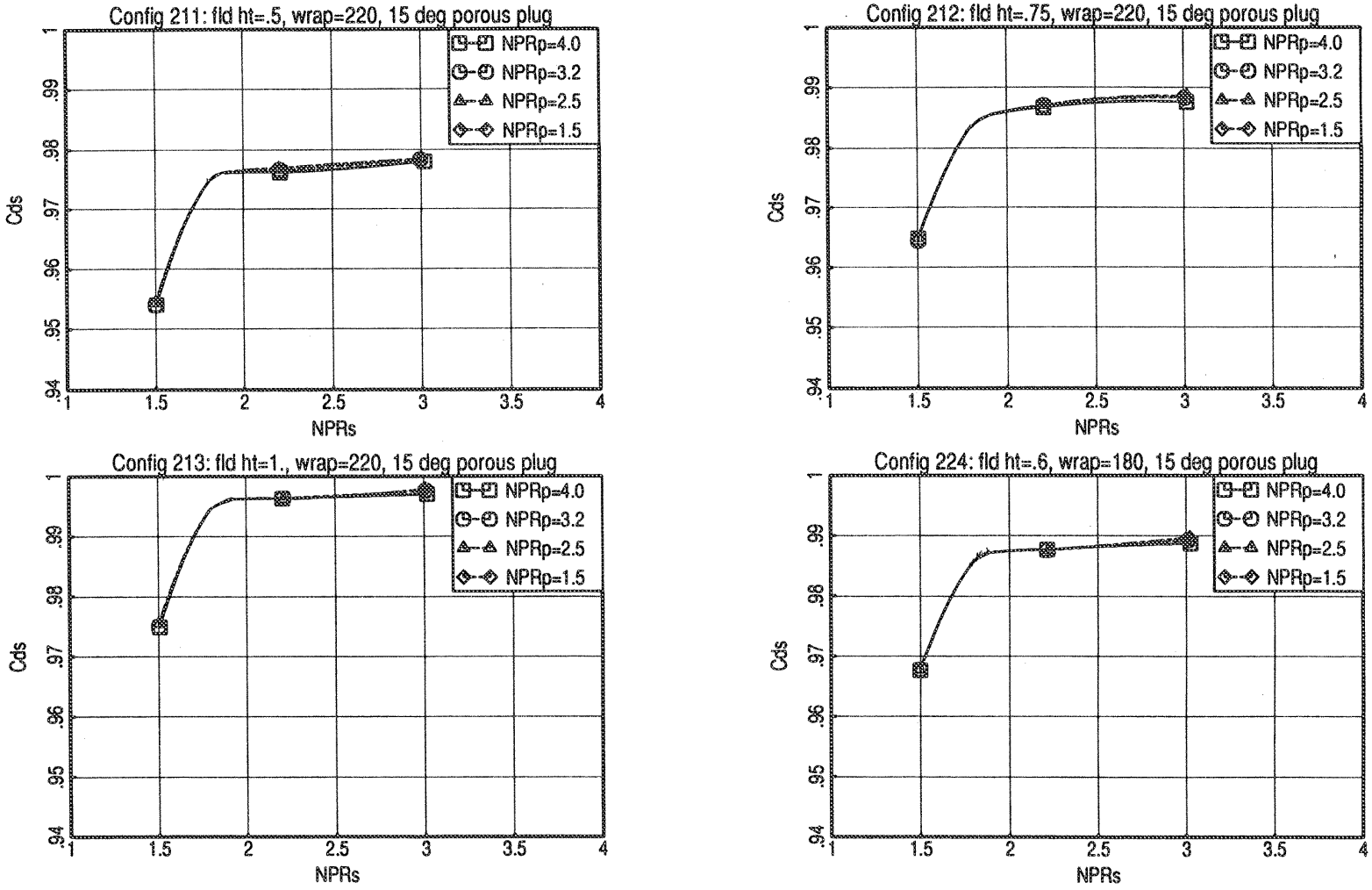

b) 15° Porous Plug Configurations

Figure 14. Continued.

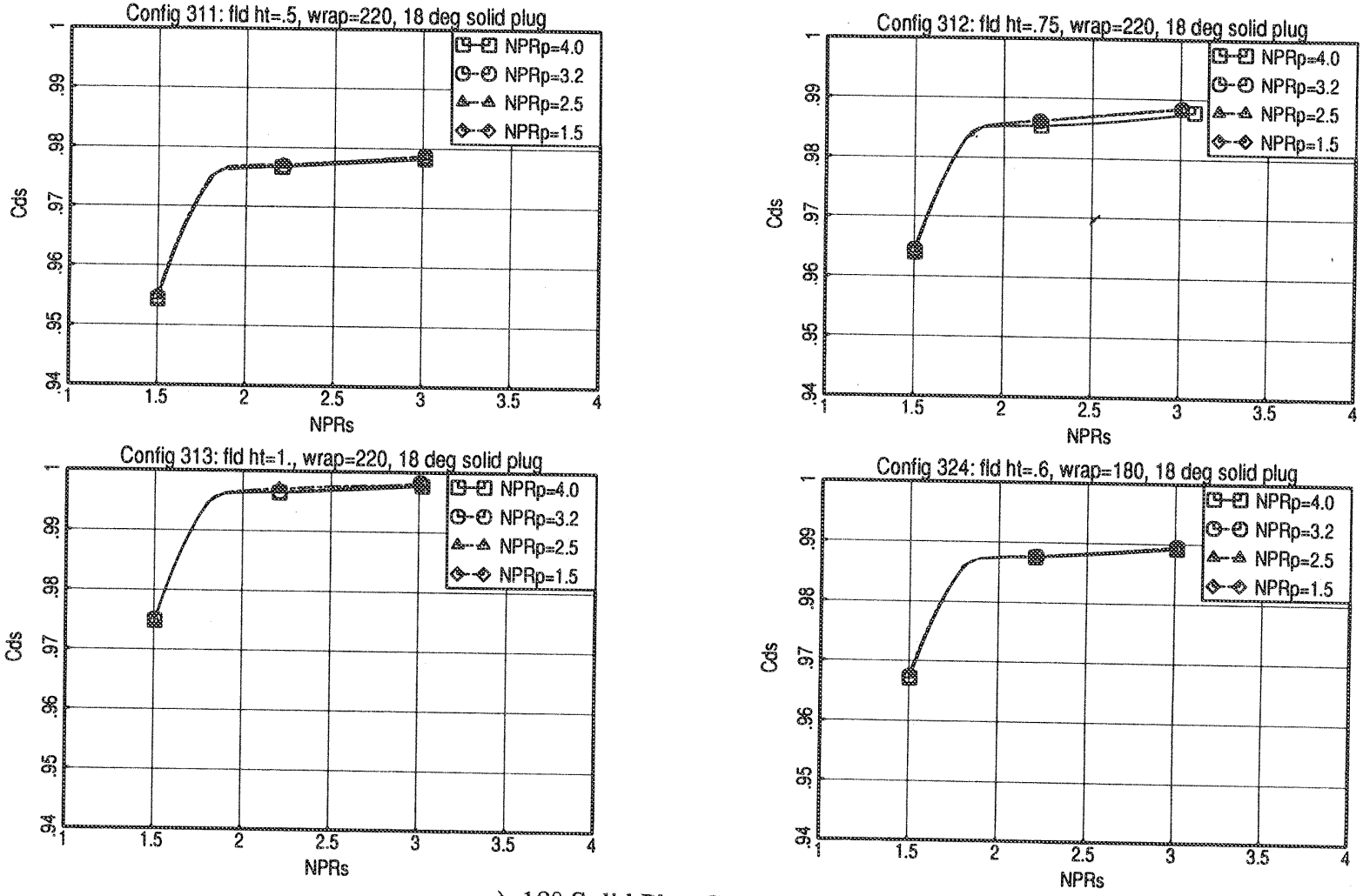

c) 18° Solid Plug Configurations

Figure 14. Concluded.

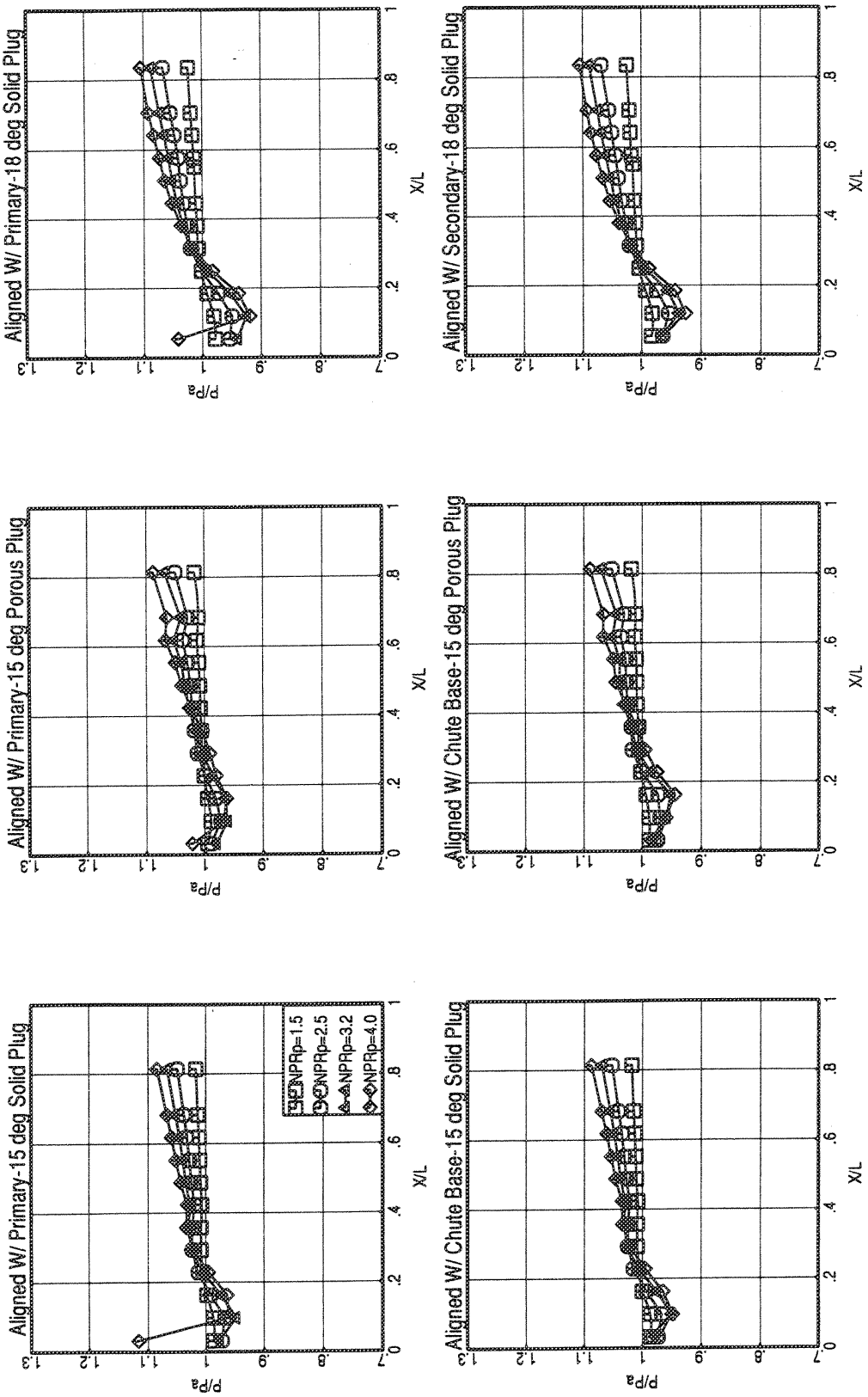

Figure 15. Variation Of Plug Static Pressure Distributions with Primary Nozzle Pressure Ratio, Wrap Angle 220°, fld ht 0.5 in, Shield Off (NPRs=1.0).

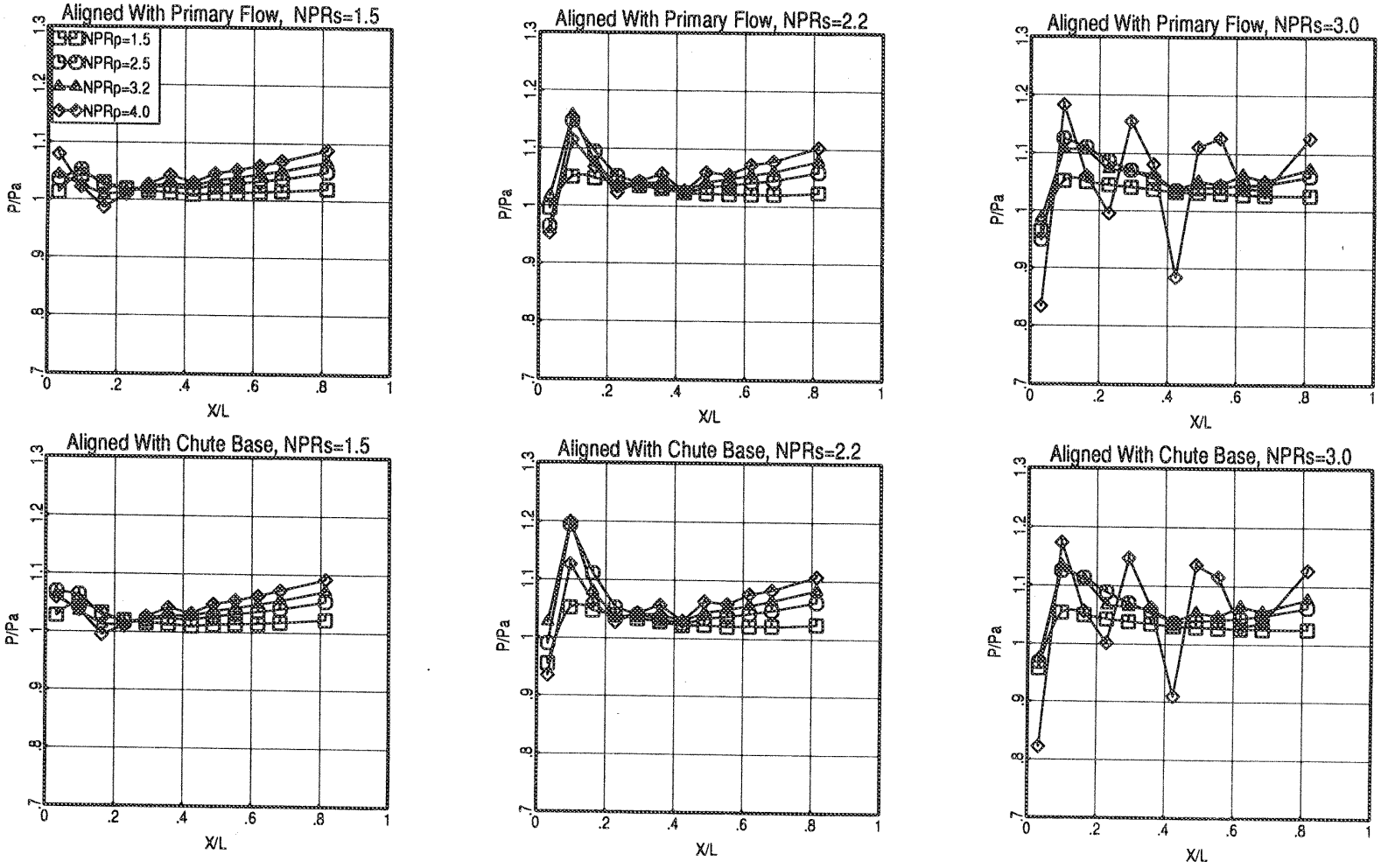

a) 15° Solid Plug, 220° Wrap, 0.5 in fld ht – Configuration 111

Figure 16. Variation Of Plug Static Pressure Distributions with Nozzle Pressure Ratios.

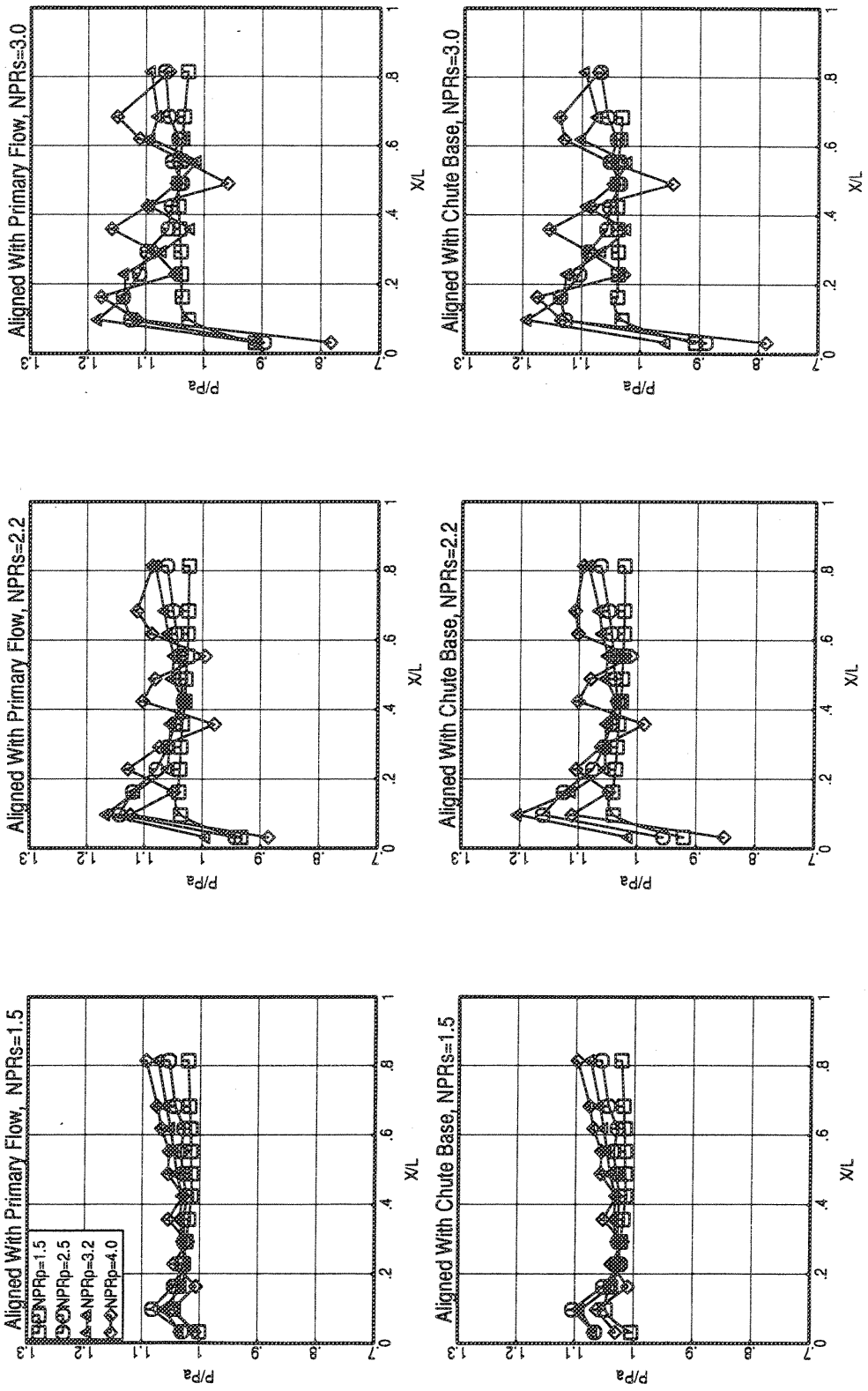

b) 15° Solid Plug, 220° Wrap, 0.75 in fld ht – Configuration 112
Figure 16. Continued.

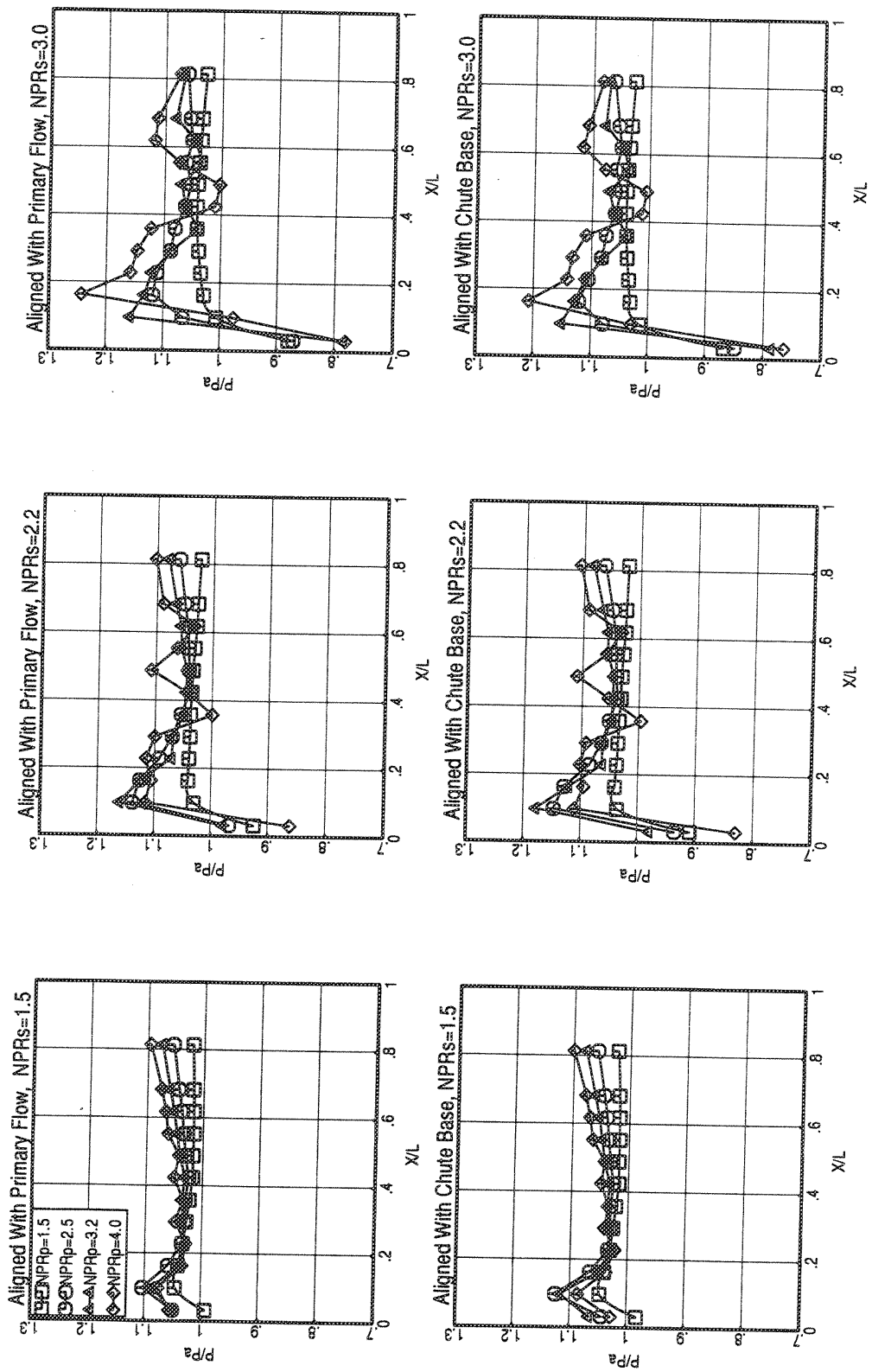

c) 15° Solid Plug, 220° Wrap, 1.0 in fld ht – Configuration 113
Figure 16. Continued.

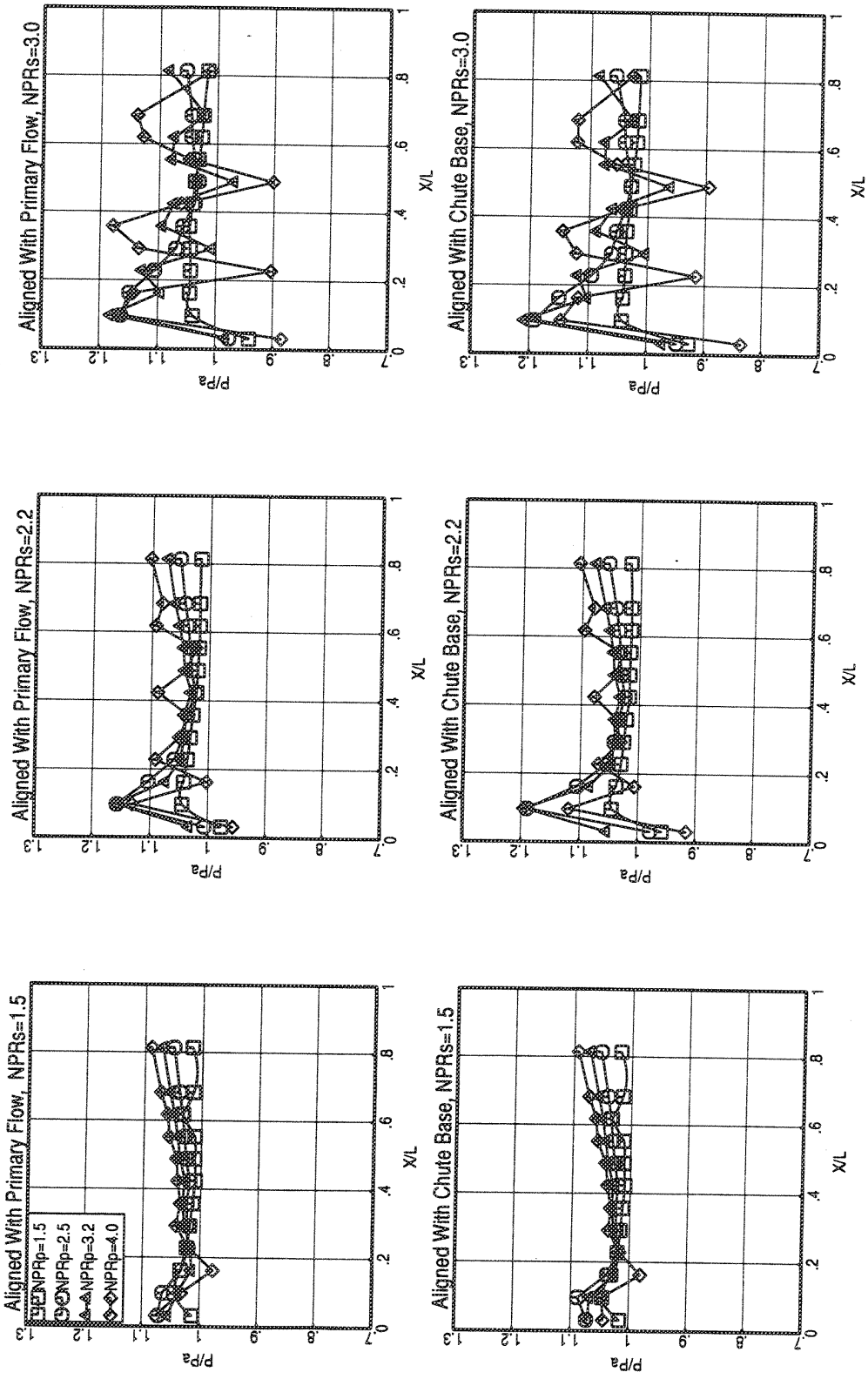

d) 15° Solid Plug, 180° Wrap, 0.6 in fld ht – Configuration 124
Figure 16. Continued.

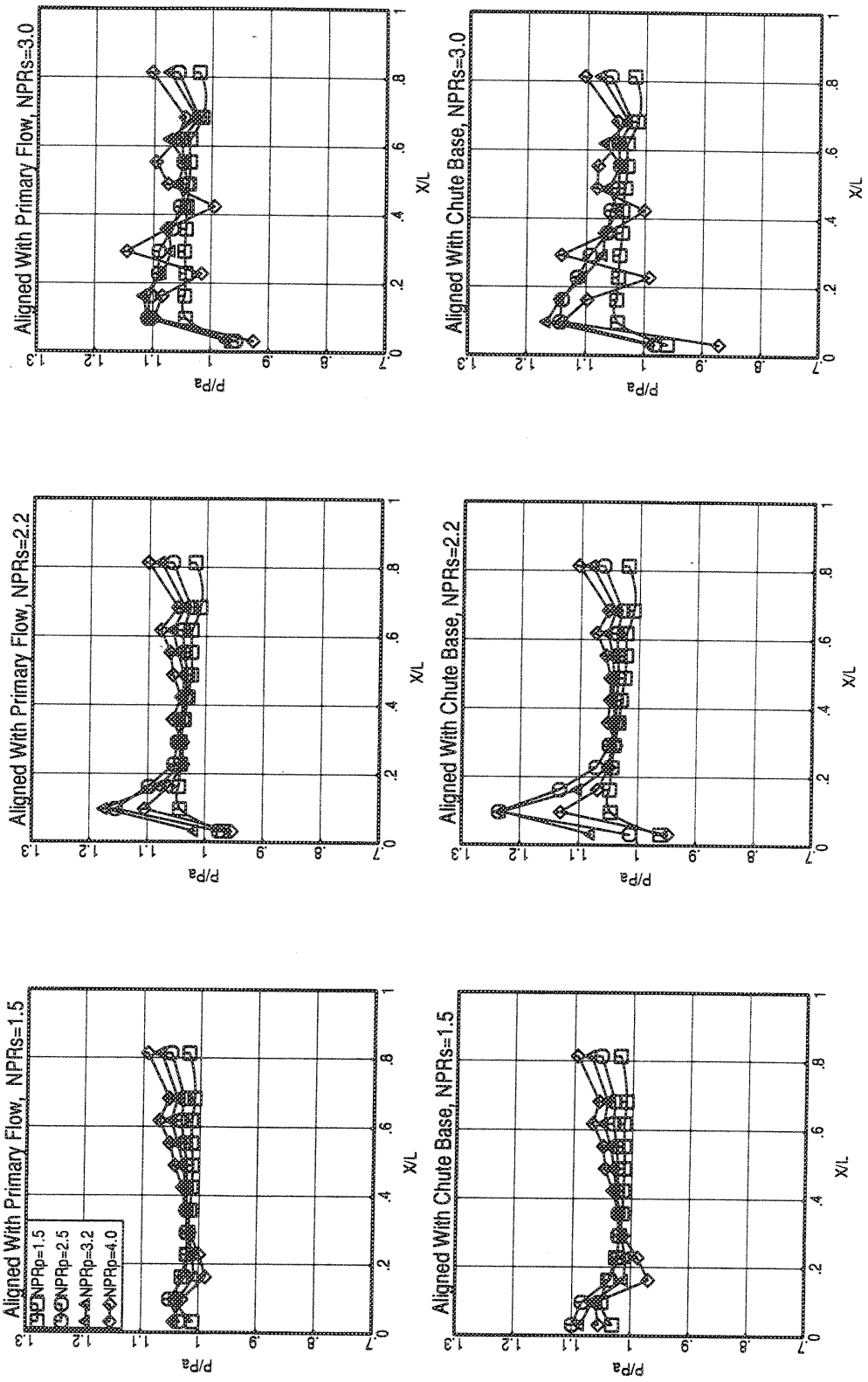

e) 15° Porous Plug, 220° Wrap, 0.5 in fld ht – Configuration 211
Figure 16. Continued.

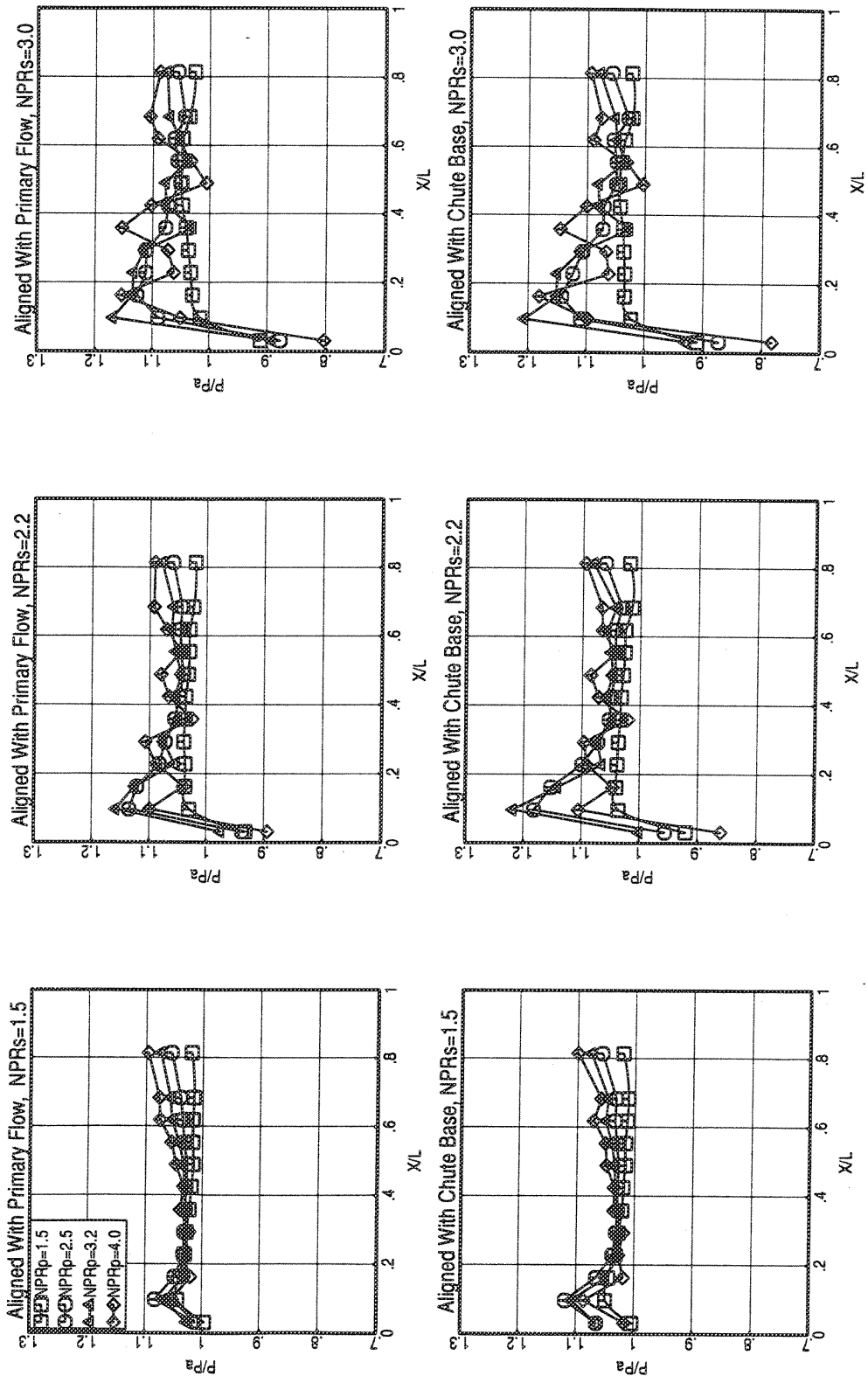

f) 15° Porous Plug, 220° Wrap, 0.75 in fld ht – Configuration 212
Figure 16. Continued.

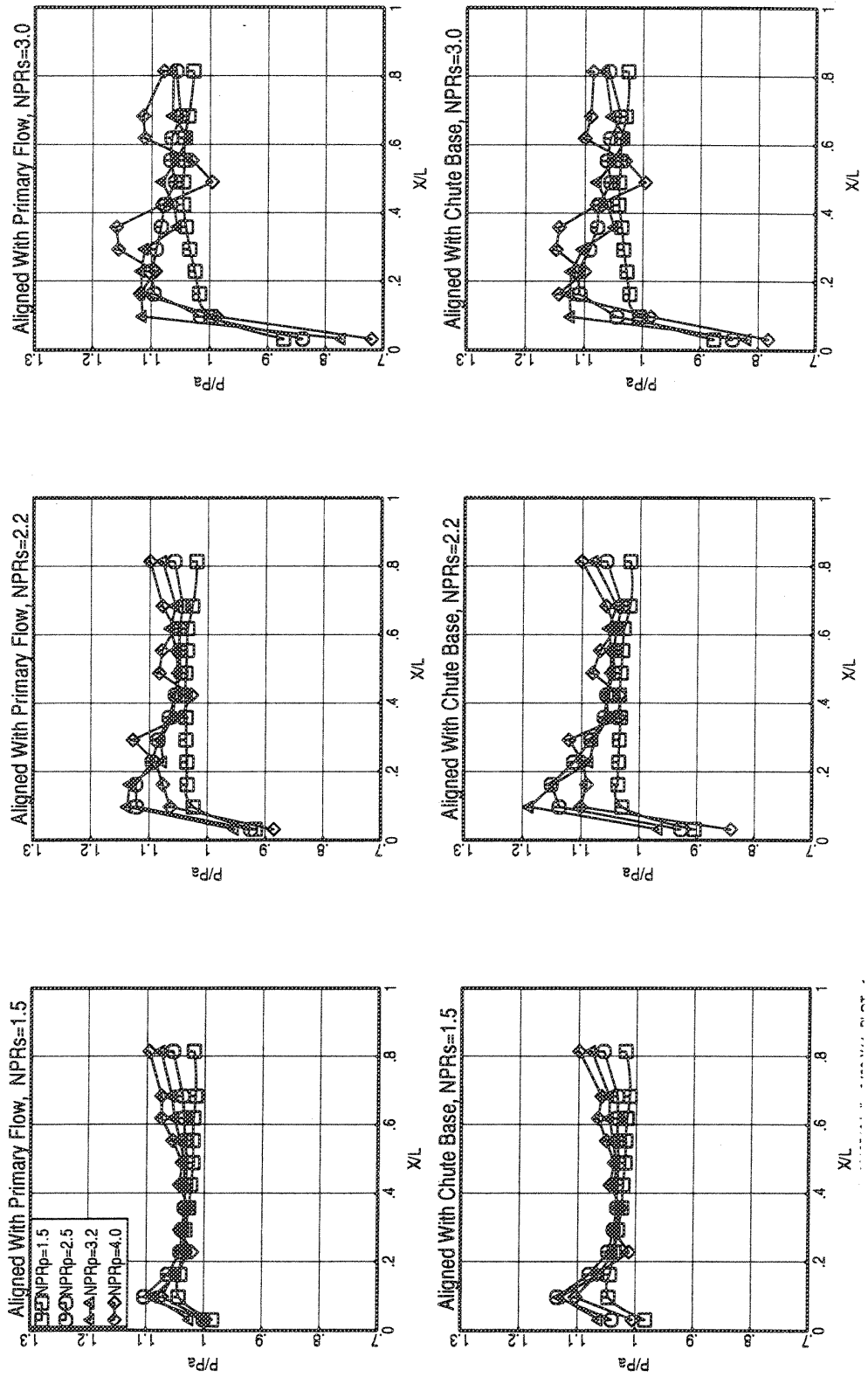

g) 15° Porous Plug, 220° Wrap, 1.0 in fld ht – Configuration 213
Figure 16. Continued.

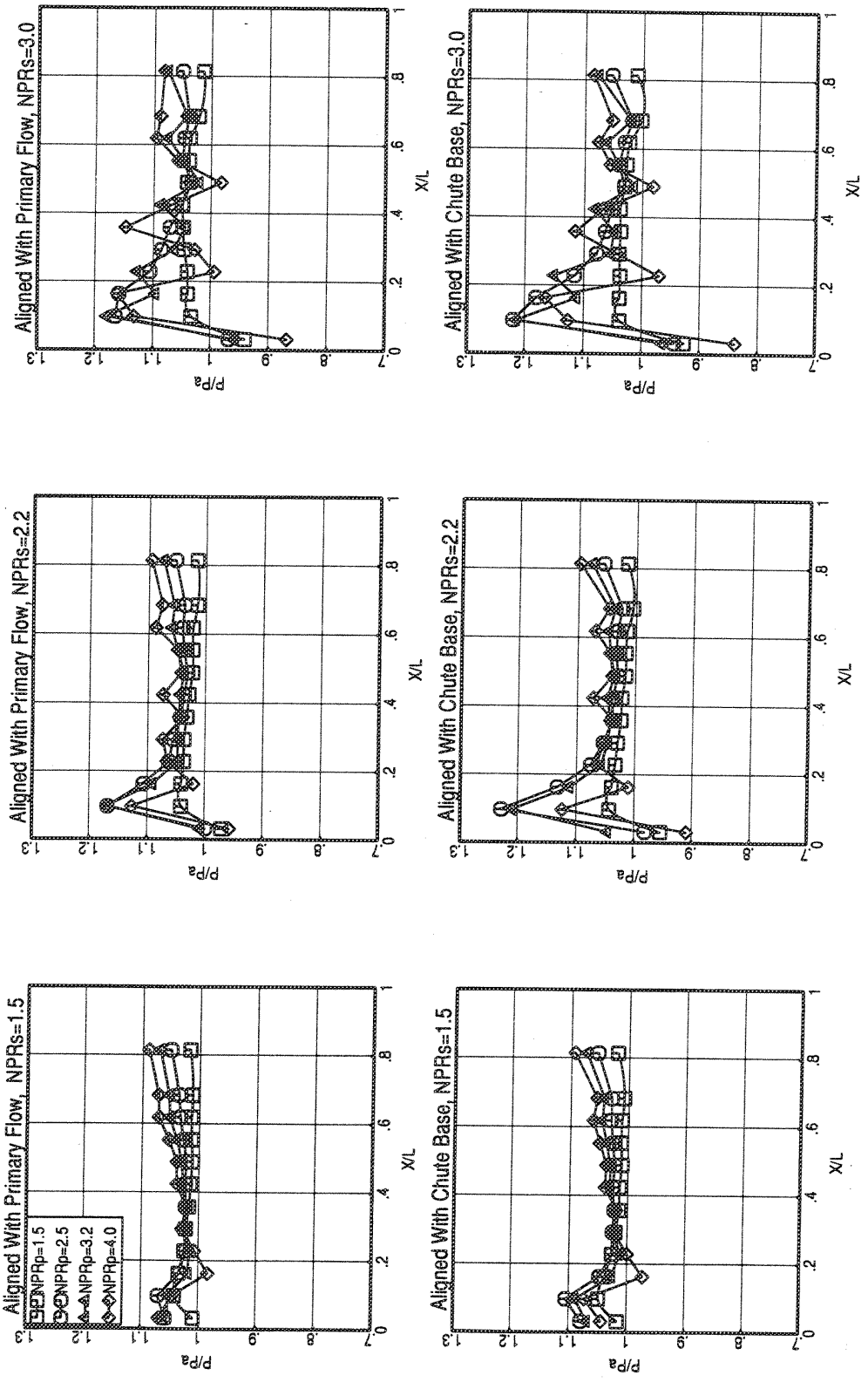

h) 15° Porous Plug, 180° Wrap, 0.6 in fld ht -- Configuration 224
Figure 16. Continued.

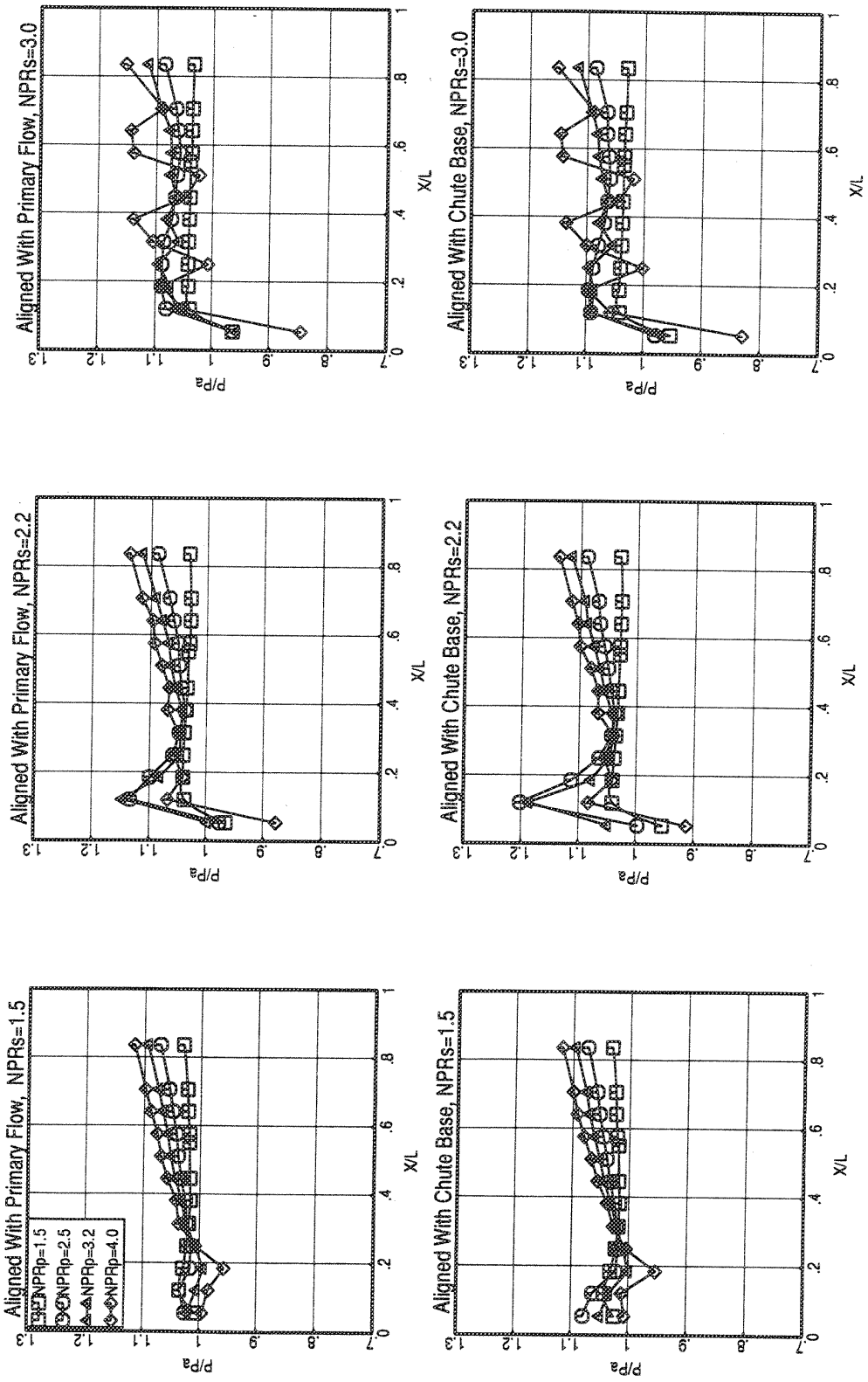

i) 18° Solid Plug, 220° Wrap, 0.5 in fld ht – Configuration 311
Figure 16. Continued.

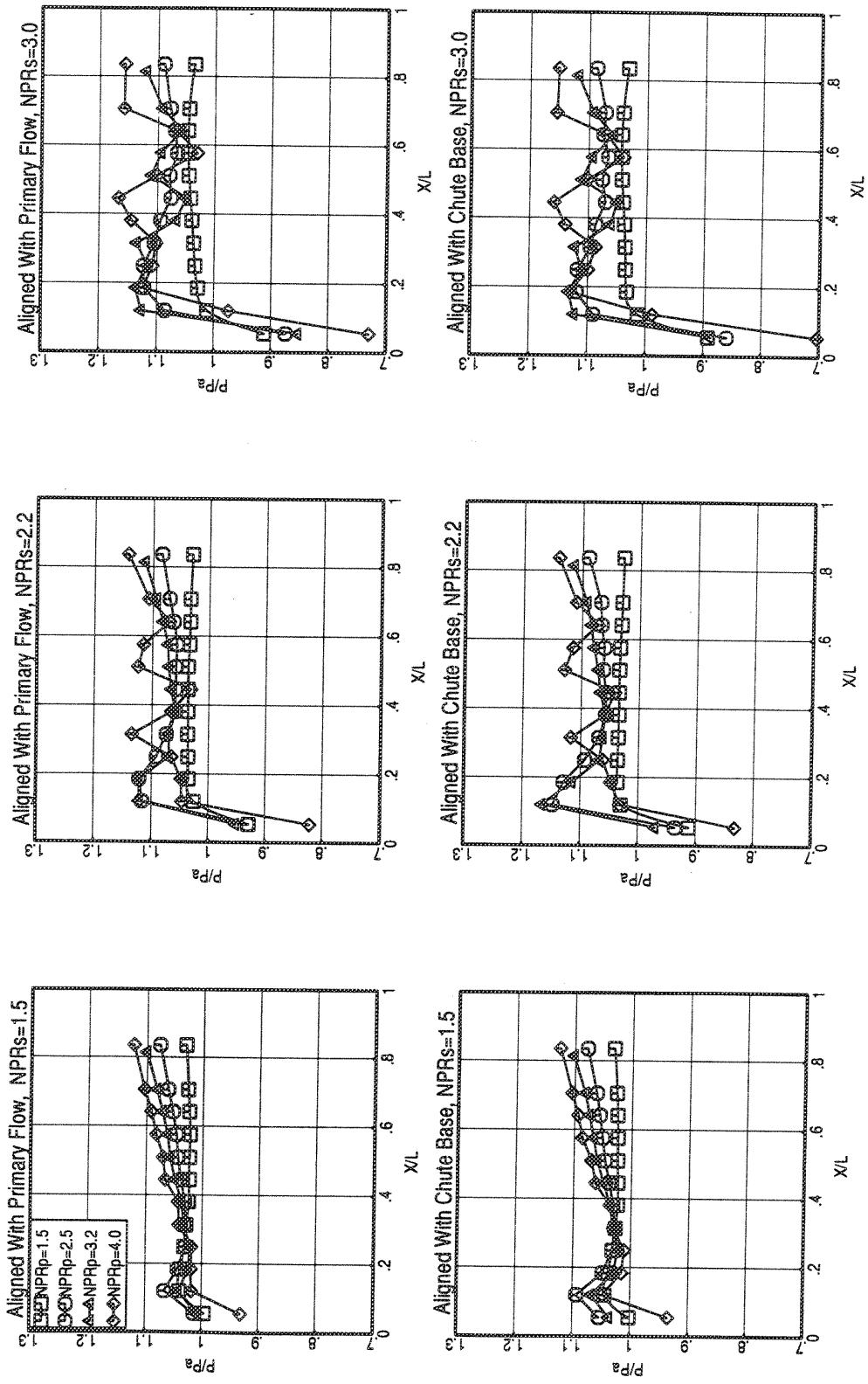

j) 18° Solid Plug, 220° Wrap, 0.75 in fld ht – Configuration 312
Figure 16. Continued.

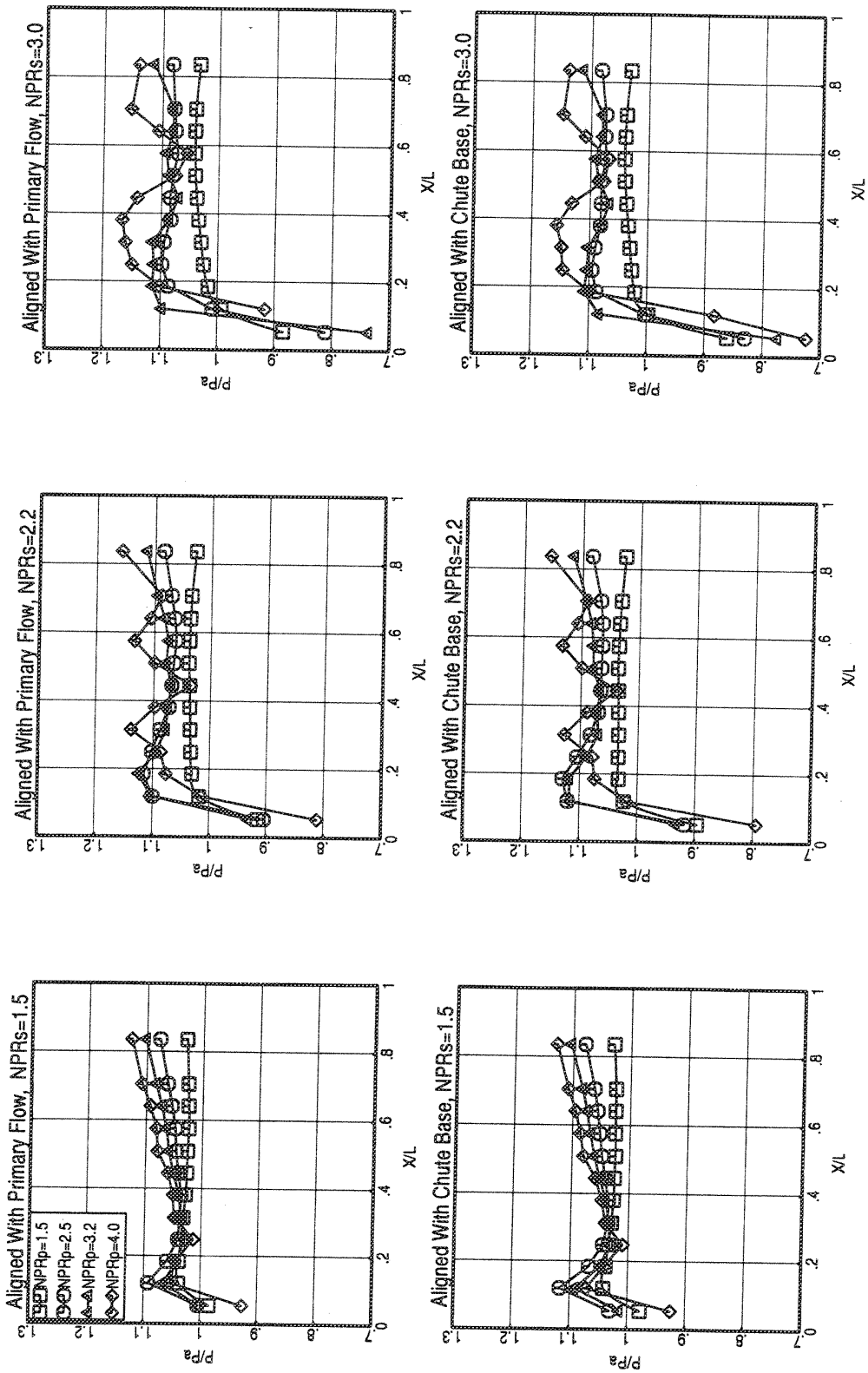

k) 18° Solid Plug, 220° Wrap, 1.0 in fld ht – Configuration 313
Figure 16. Continued.

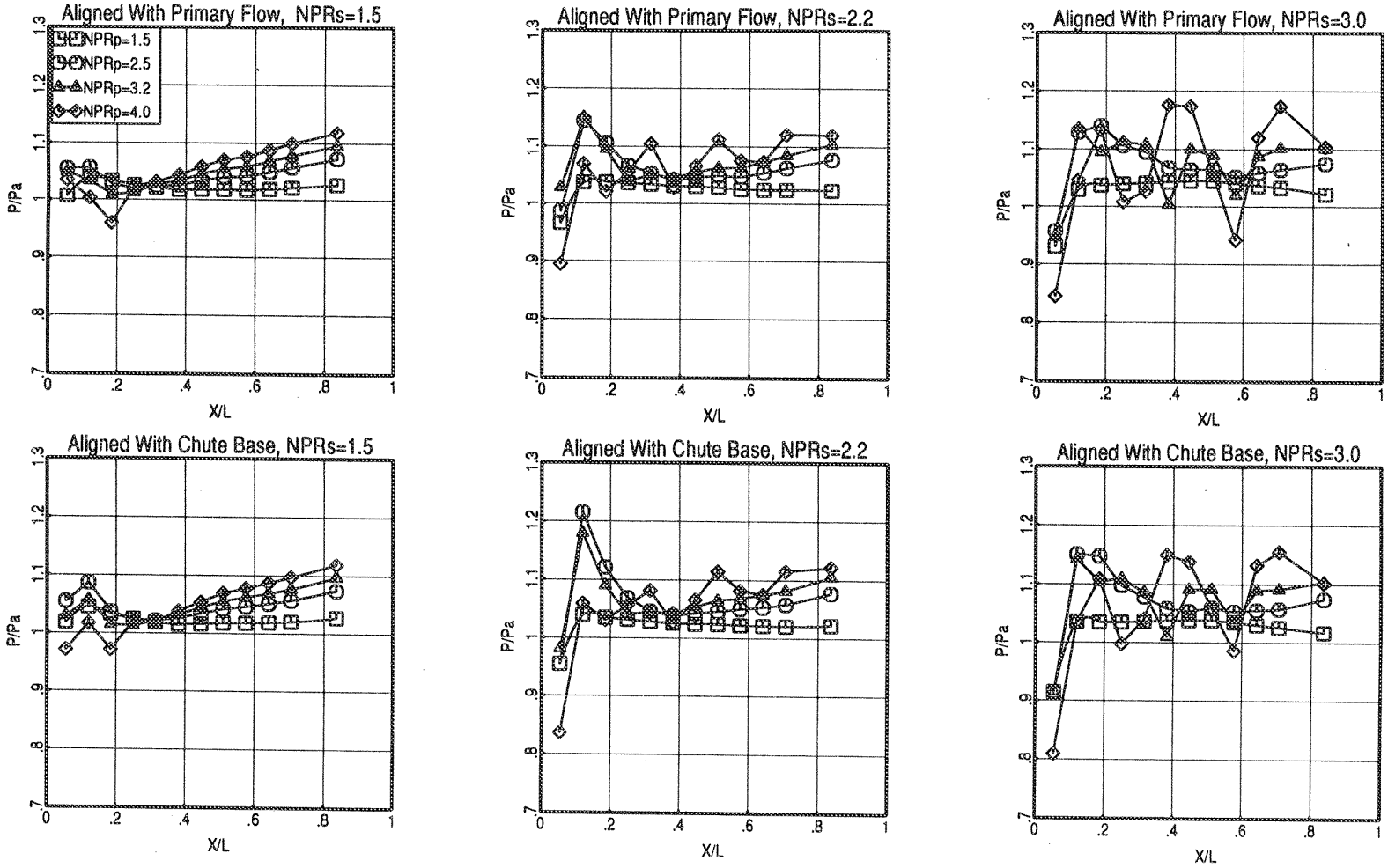

l) 18° Solid Plug, 180° Wrap, 0.6 in fld ht – Configuration 324
Figure 16. Concluded.

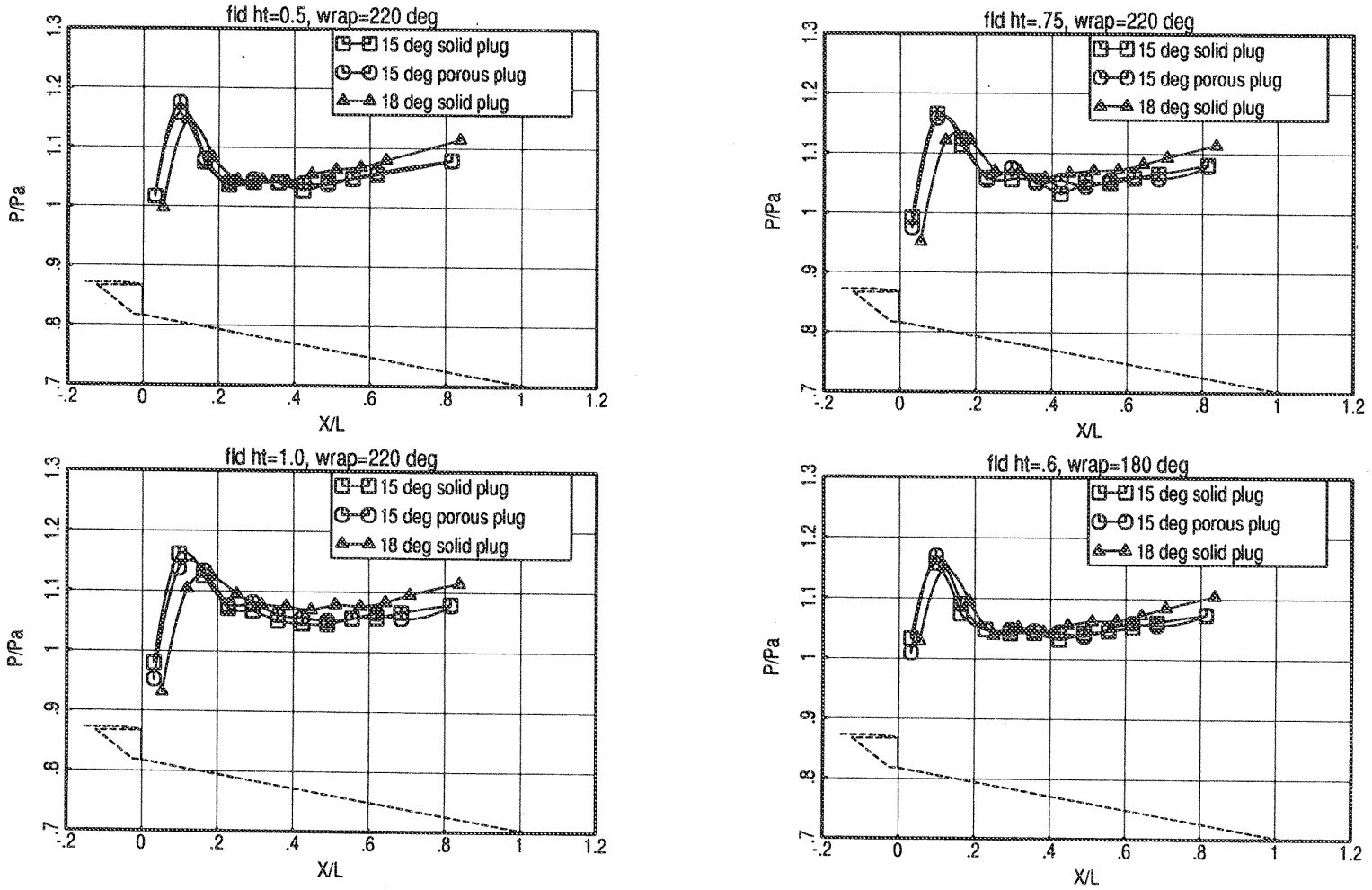

a) Row Aligned With Primary Flow

Figure 17. Configuration Comparison Of Plug Static Pressure Distributions; @ NPRp=3.2, NPRs=2.2.

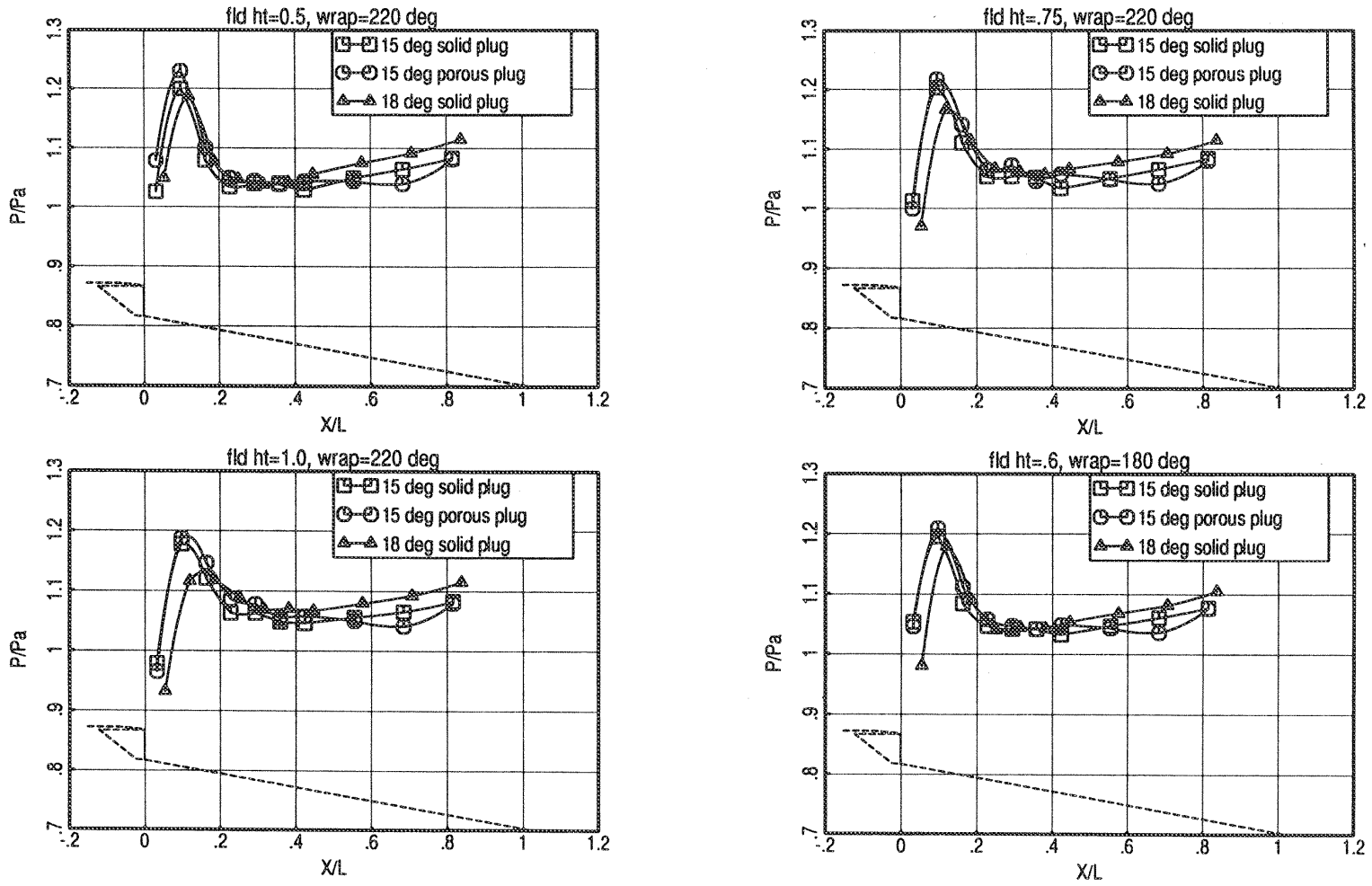

b) Row Aligned With Chute Base

Figure 17. Concluded.

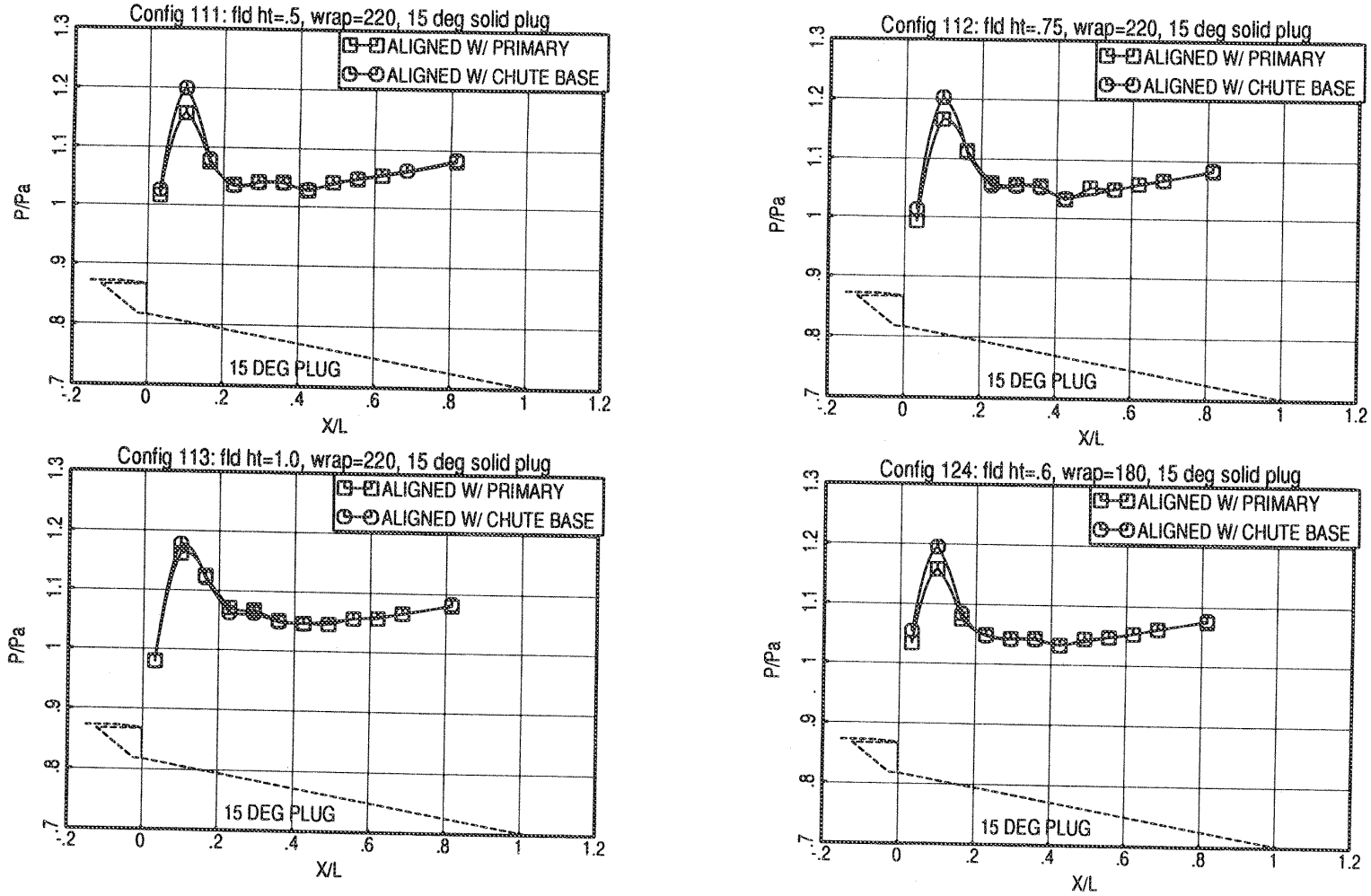

a) 15° Solid Plug Configurations.

Figure 18. Row Comparison Of Plug Static Pressure Distributions, @ NPRp=3.2, NPRs=2.2.

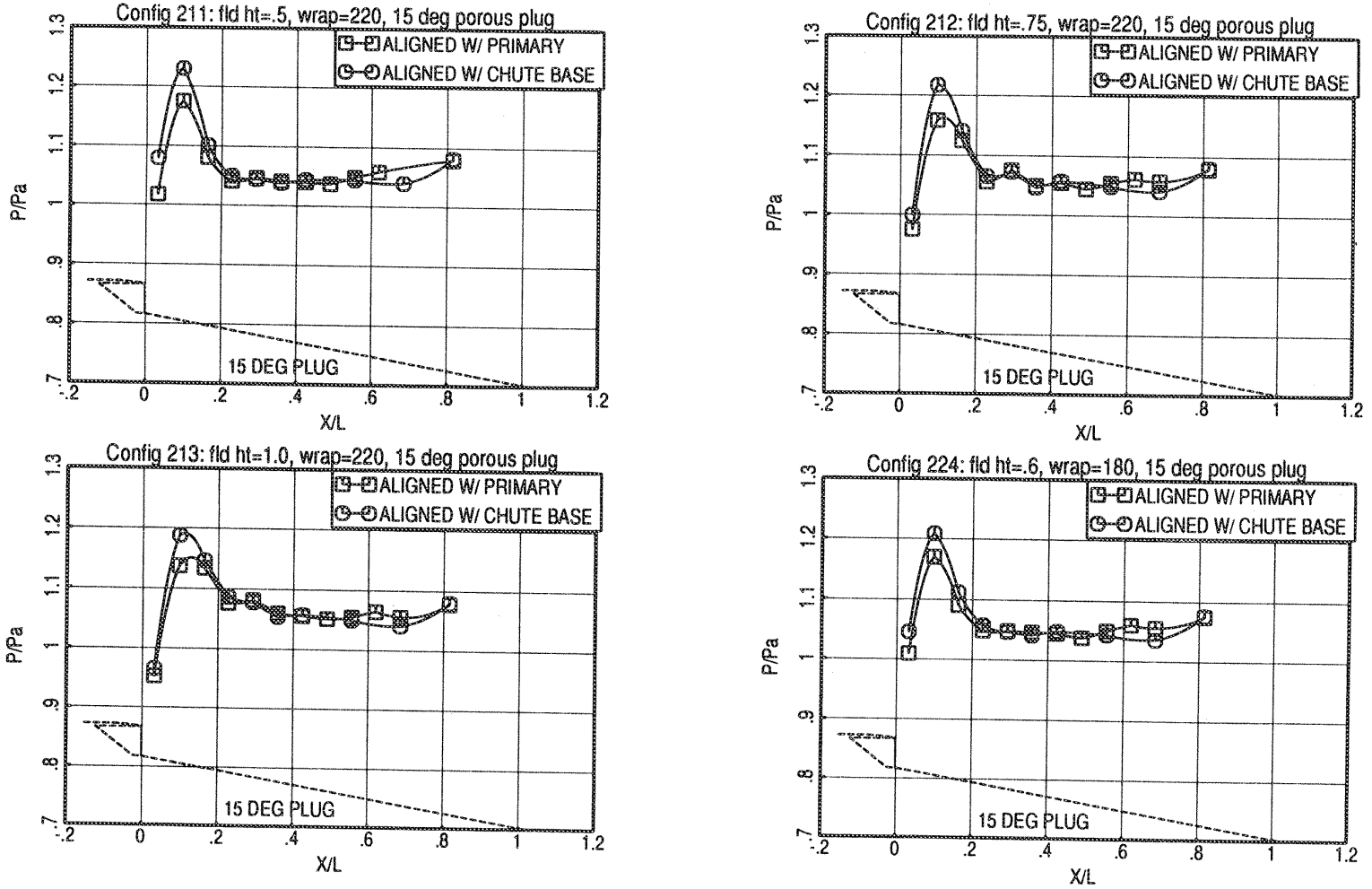

b) 15° Porous Plug Configurations.
Figure 18. Continued

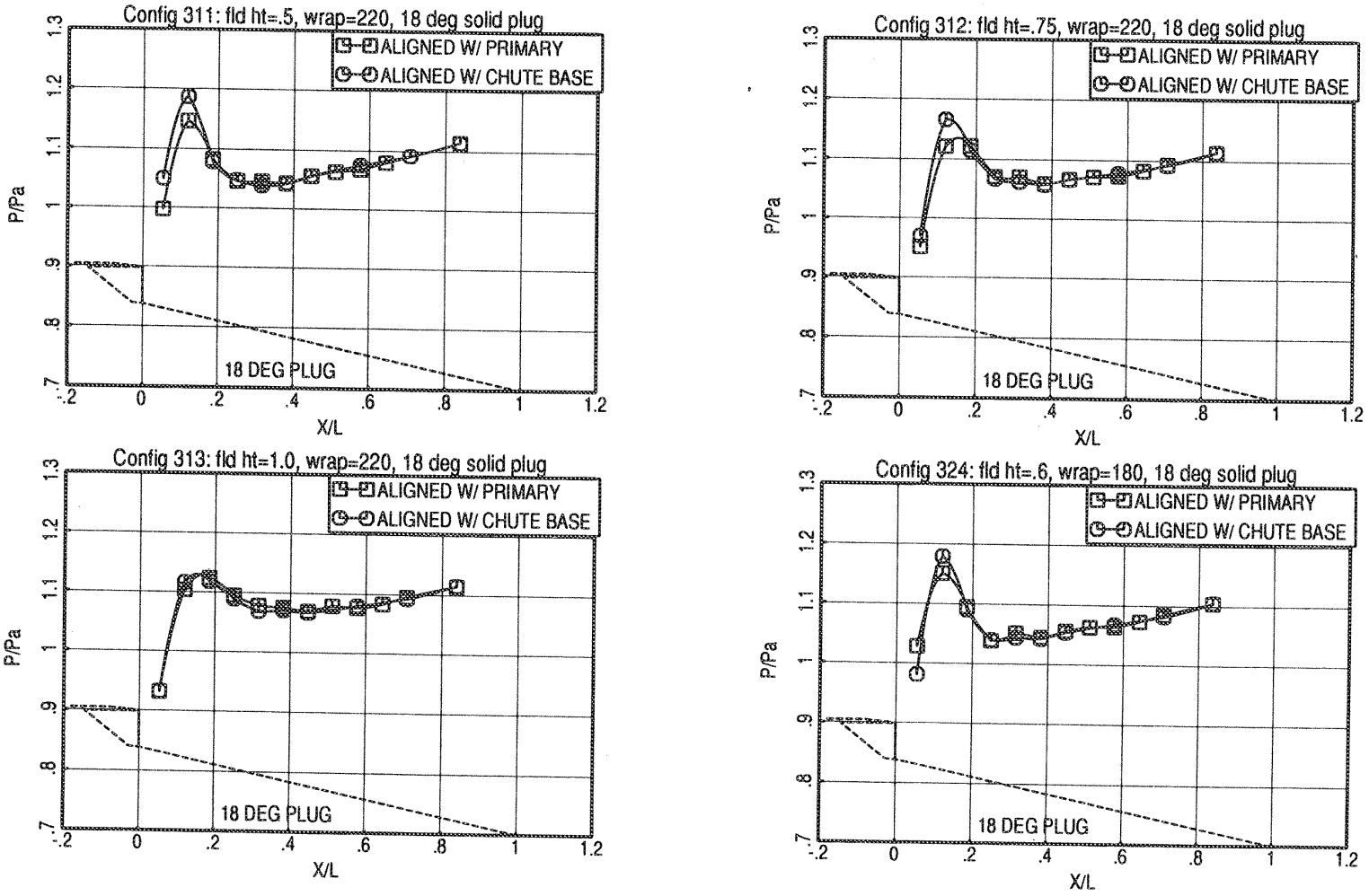

c) 18° Solid Plug Configurations.

Figure 18. Concluded.

REPORT DOCUMENTATION PAGE

Form Approved
OMB No. 0704-0188

1. AGENCY USE ONLY (*Leave blank*)	2. REPORT DATE	3. REPORT TYPE AND DATES COVERED
	January 2005	Final Contractor Report

4. TITLE AND SUBTITLE

Static Aerodynamic Performance Investigation of a Fluid Shield Nozzle

5. FUNDING NUMBERS

WBS–22–714–09–46
NAS3–25951

6. AUTHOR(S)

C. Balan and J.W. Askew

7. PERFORMING ORGANIZATION NAME(S) AND ADDRESS(ES)

General Electric Aircraft Engines
One Neumann Way
Cincinnati, Ohio 45125

8. PERFORMING ORGANIZATION REPORT NUMBER

E–14781

9. SPONSORING/MONITORING AGENCY NAME(S) AND ADDRESS(ES)

National Aeronautics and Space Administration
Washington, DC 20546–0001

10. SPONSORING/MONITORING AGENCY REPORT NUMBER

NASA CR—2005-213321

11. SUPPLEMENTARY NOTES

This research was originally published internally as HSR027 in May 1996. Responsible person, Diane Chapman, Ultra-Efficient Engine Technology Program Office, NASA Glenn Research Center, organization code PA, 216–433–2309.

12a. DISTRIBUTION/AVAILABILITY STATEMENT

Unclassified - Unlimited
Subject Categories: 01, 05, and 07 Distribution: Nonstandard

Available electronically at http://gltrs.grc.nasa.gov

This publication is available from the NASA Center for AeroSpace Information, 301–621–0390.

12b. DISTRIBUTION CODE

13. ABSTRACT ***(Maximum 200 words)***

In pursuit of an acoustically acceptable, high performance exhaust system capable of meeting Federal Aviation Regulation 36—Stage 3 noise goals for the High Speed Civil Transport application, General Electric Aircraft Engines conducted a design study to incorporate a fluid shield into a 36-chute suppressor exhaust-nozzle system. After a full scale preliminary mechanical design of the resulting fluid shield exhaust system, scale model aerodynamic performance tests and acoustic tests were conducted to establish both aerodynamic performance and acoustic characteristics. Data are presented as thrust coefficients, discharge coefficients, chute-base pressure drags, and plug static pressure distributions.

14. SUBJECT TERMS

High speed civil transport; Fluid shield; Exhaust-nozzle system

15. NUMBER OF PAGES

72

16. PRICE CODE

17. SECURITY CLASSIFICATION OF REPORT	18. SECURITY CLASSIFICATION OF THIS PAGE	19. SECURITY CLASSIFICATION OF ABSTRACT	20. LIMITATION OF ABSTRACT
Unclassified	Unclassified	Unclassified	